
Neural Multi-Objective Combinatorial Optimization with Diversity Enhancement

Jinbiao Chen¹, Zizhen Zhang¹, Zhiguang Cao², Yaoxin Wu³, Yining Ma⁴,
Te Ye¹, and Jiahai Wang^{1,5,6,*}

¹School of Computer Science and Engineering, Sun Yat-sen University, P.R. China

²School of Computing and Information Systems, Singapore Management University, Singapore

³Department of Industrial Engineering & Innovation Sciences,
Eindhoven University of Technology, Netherlands

⁴Department of Industrial Systems Engineering & Management,
National University of Singapore, Singapore

⁵Key Laboratory of Machine Intelligence and Advanced Computing, Ministry of Education,
Sun Yat-sen University, P.R. China

⁶Guangdong Key Laboratory of Big Data Analysis and Processing, Guangzhou, P.R. China
chenjb69@mail2.sysu.edu.cn, zhangzzh7@mail.sysu.edu.cn
zgcao@smu.edu.sg, y.wu2@tue.nl, yiningma@nus.edu
yete@mail2.sysu.edu.cn, wangjiah@mail.sysu.edu.cn

Abstract

Most of existing neural methods for multi-objective combinatorial optimization (MOCO) problems solely rely on decomposition, which often leads to repetitive solutions for the respective subproblems, thus a limited Pareto set. Beyond decomposition, we propose a novel neural heuristic with diversity enhancement (NHDE) to produce more Pareto solutions from two perspectives. On the one hand, to hinder duplicated solutions for different subproblems, we propose an indicator-enhanced deep reinforcement learning method to guide the model, and design a heterogeneous graph attention mechanism to capture the relations between the instance graph and the Pareto front graph. On the other hand, to excavate more solutions in the neighborhood of each subproblem, we present a multiple Pareto optima strategy to sample and preserve desirable solutions. Experimental results on classic MOCO problems show that our NHDE is able to generate a Pareto front with higher diversity, thereby achieving superior overall performance. Moreover, our NHDE is generic and can be applied to different neural methods for MOCO.

1 Introduction

Multi-objective combinatorial optimization (MOCO) has been extensively studied in the communities of computer science and operations research [1, 2]. It also commonly exists in many industries, such as transportation [3], manufacturing [4], energy [5], and telecommunication [6]. MOCO features multiple conflicting objectives based on NP-hard combinatorial optimization (CO), practical yet more complex. Rather than finding an optimal solution like in the single-objective optimization, MOCO pursues a set of Pareto-optimal solutions, called *Pareto set*, to trade-off the multiple objectives. In general, a decent Pareto set is captured by both desirable convergence (optimality) and diversity.

Since exactly solving MOCO may require exponentially increasing computational time [7], the heuristic methods [8] have been favored in practice over the past few decades, which aim to yield an

*Corresponding Author.

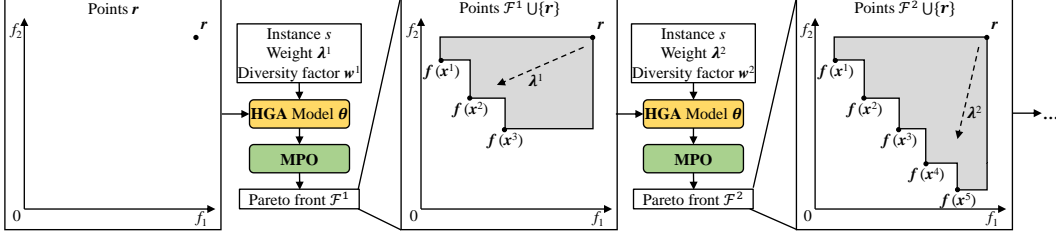


Figure 1: The framework of NHDE. For subproblem i , the heterogeneous graph attention (HGA) model takes instance s , points $\mathcal{F}^{i-1} \cup \{r\}$, weight λ^i , and diversity factor w^i as inputs, and generates solutions to optimize the scalar objective and hypervolume (size of the gray area). More solutions are sampled and the Pareto front \mathcal{F}^i is then efficiently updated based on multiple Pareto optima (MPO).

approximate Pareto set. Despite a relatively high efficiency, heuristic methods need domain-specific knowledge and massive iterative search. As *neural CO* methods based on deep reinforcement learning (DRL) recently achieved notable success in CO problems such as routing, scheduling, and bin packing [9–12], a number of *neural MOCO* methods have also been accordingly developed [13–16]. Typically, parameterized as a deep model, Neural MOCO is able to automatically learn a heuristic (or policy), so as to directly construct near-optimal solutions in an end-to-end fashion, which takes much less computational time than the traditional ones.

Existing neural MOCO methods mostly decompose an MOCO problem into a series of single-objective CO subproblems and derive a Pareto set by solving them. However, while enjoying a favorable efficiency for neural MOCO, the sole decomposition is less effective in finding as many diverse solutions as possible, since constructing an optimal solution for the decomposed subproblems is always carried out independently, causing repetitive or duplicated ones for different subproblems.

To tackle this issue, we propose a neural heuristic with diversity enhancement (NHDE), as illustrated in Figure 1. Distinguished from existing neural methods, NHDE couples the decomposition with a comprehensive indicator to learn a policy that can produce diverse solutions across the subproblems while further improving the performance. Besides, for a given subproblem, multiple relevant solutions, rather than a single optimal solution with respect to the scalar objective, are found based on a proposed multiple Pareto optima (MPO) strategy, so as to further strengthen the diversity.

Our contributions are summarized as follows. (1) We propose an indicator-enhanced DRL method. To encourage the deep model to generate different yet diverse solutions for decomposed subproblems, NHDE inputs the Pareto front composed of the preceding solutions and introduces an indicator comprehensively measuring convergence and diversity in the reward. (2) We design a heterogeneous graph attention model to effectively capture the correlation between an instance graph and its Pareto front graph. (3) We present a multiple Pareto optima (MPO) strategy to further identify more relevant solutions in the neighborhood of each subproblem and efficiently update the Pareto front. (4) We deploy our NHDE with two different types of neural MOCO methods to demonstrate its versatility. Experimental results based on various MOCO problems show that our NHDE outperforms state-of-the-art neural baselines, especially with significant improvement in the diversity.

2 Related works

Exact and heuristic methods for MOCO. Exact methods [7, 17] for MOCO can attain the accurate Pareto set, but their computational time may grow exponentially, rendering them less practical. As an alternative, heuristic methods such as multi-objective evolutionary algorithms (MOEAs) have gained widespread attention in practice. Dominance-based NSGA-II [18], decomposition-based MOEA/D [19], and indicator-based SMS-EMOA [20] are three typical paradigms of MOEAs. In these MOEAs, local search, a crucial technique specialized to the target CO, is usually employed [21–23].

Neural CO. In the past few years, neural *construction* methods [24–26] were proposed to rapidly yield high-quality solutions in an end-to-end fashion. A well-known representative is *Attention Model* (AM) [27], which was developed based on the *Transformer* architecture [28]. Then, AM inspired a large number of subsequent works [29–35], which further boosted the performance. Among them,

the policy optimization with multiple optima (POMO) [36], leveraging the solution and problem symmetries, is recognized as a prominent approach. Besides, the other line of works, known as neural *improvement* methods [37–41], exploited DRL to assist the iterative improvement process from an initial but complete solution, following a learn-to-improve paradigm.

Neural MOCO. Decomposition is a mainstream scheme in learning-based methods for multi-objective optimization [42–44]. An MOCO problem can be decomposed into a series of single-objective CO problems and then solved by neural construction methods to approximate the Pareto set. A couple of preliminary works trained multiple deep models with transfer learning [13, 45], where each deep model coped with one subproblem. Evolutionary learning [46, 47] was introduced to evolve deep models to further improve the performance. Instead of training multiple deep models for preset weights, preference-conditioned multi-objective combinatorial optimization (PMOCO) [14] and Meta-DRL (MDRL) [15], both of which only trained one deep model, were more flexible and practical. For a given weight vector, the former used a hypernetwork to derive the decoder parameters to solve the corresponding subproblem, while the latter rapidly fine-tuned a pre-trained meta-model to solve the corresponding subproblem. However, those solely decomposition-based neural MOCO methods are limited in the diversity with respect to the solutions of the Pareto set, since some subproblems may lead to duplicated solutions, especially when they are solved independently.

3 Preliminary

3.1 MOCO

An MOCO problem with M objectives can be expressed as $\min_{\mathbf{x} \in \mathcal{X}} \mathbf{f}(\mathbf{x}) = (f_1(\mathbf{x}), f_2(\mathbf{x}), \dots, f_M(\mathbf{x}))$, where \mathcal{X} is a set of discrete decision variables.

Definition 1 (Pareto dominance). A solution $\mathbf{x}^1 \in \mathcal{X}$ dominates another solution $\mathbf{x}^2 \in \mathcal{X}$ ($\mathbf{x}^1 \prec \mathbf{x}^2$), if and only if $f_i(\mathbf{x}^1) \leq f_i(\mathbf{x}^2), \forall i \in \{1, \dots, M\}$ and $\exists j \in \{1, \dots, M\}, f_j(\mathbf{x}^1) < f_j(\mathbf{x}^2)$.

Definition 2 (Pareto optimality). A solution $\mathbf{x}^* \in \mathcal{X}$ is Pareto-optimal if it is not dominated by any other solution, i.e., $\nexists \mathbf{x}' \in \mathcal{X}$ such that $\mathbf{x}' \prec \mathbf{x}^*$.

Definition 3 (Pareto set/front). MOCO aims to uncover a Pareto set, comprising all Pareto optimal solutions $\mathcal{P} = \{\mathbf{x}^* \in \mathcal{X} \mid \nexists \mathbf{x}' \in \mathcal{X} : \mathbf{x}' \prec \mathbf{x}^*\}$. The Pareto front $\mathcal{F} = \{\mathbf{f}(\mathbf{x}) \mid \mathbf{x} \in \mathcal{P}\}$ corresponds to the objective values of Pareto set, with each $\mathbf{f}(\mathbf{x})$ referred to as a *point* in the objective space.

3.2 Decomposition

For MOCO, decomposition [19] is a prevailing scheme due to its flexibility and effectiveness. An MOCO problem can be decomposed into N subproblems with N weights. Each subproblem is a single-objective CO problem via scalarization $g(\mathbf{x}|\boldsymbol{\lambda})$ with a weight $\boldsymbol{\lambda} \in \mathcal{R}^M$ satisfying $\lambda_m \geq 0$ and $\sum_{m=1}^M \lambda_m = 1$. The Pareto set then can be derived by solving the N subproblems.

The simplest yet effective decomposition approach is the weighted sum (WS). It uses the linear scalarization of M objectives, which hardly raises the complexity of the subproblems, as follows,

$$\min_{\mathbf{x} \in \mathcal{X}} g_{\text{ws}}(\mathbf{x}|\boldsymbol{\lambda}) = \sum_{m=1}^M \lambda_m f_m(\mathbf{x}). \quad (1)$$

3.3 Indicator

Hypervolume (HV) is a mainstream indicator to measure performance, as it can comprehensively assess the convergence and diversity without the exact Pareto front [48]. For a Pareto front \mathcal{F} in the objective space, $\text{HV}_{\mathbf{r}}(\mathcal{F})$ with respect to a fixed reference point $\mathbf{r} \in \mathcal{R}^M$ is defined as follows,

$$\text{HV}_{\mathbf{r}}(\mathcal{F}) = \mu \left(\bigcup_{\mathbf{f}(\mathbf{x}) \in \mathcal{F}} [\mathbf{f}(\mathbf{x}), \mathbf{r}] \right), \quad (2)$$

where μ is the Lebesgue measure, i.e., M -dimensional volume, and $[\mathbf{f}(\mathbf{x}), \mathbf{r}]$ is a M -dimensional cube, i.e., $[\mathbf{f}(\mathbf{x}), \mathbf{r}] = [f_1(\mathbf{x}), r_1] \times \dots \times [f_M(\mathbf{x}), r_M]$.

A 2-dimensional example with 5 *points* in the objective space is depicted in Figure 1, where $\mathcal{F} = \{\mathbf{f}(\mathbf{x}^1), \mathbf{f}(\mathbf{x}^2), \mathbf{f}(\mathbf{x}^3), \mathbf{f}(\mathbf{x}^4), \mathbf{f}(\mathbf{x}^5)\}$. $\text{HV}_r(\mathcal{F})$ is equal to the size of the gray area, and finally normalized into $[0, 1]$. All methods share the same reference point \mathbf{r} for a problem (see Appendix A).

4 Methodology

Our *neural heuristic with diversity enhancement* (NHDE) exploits indicator-enhanced DRL to produce diverse solutions across different subproblems and leverages a multiple Pareto optima (MPO) strategy to find multiple neighbor solutions for each subproblem, as illustrated in Figure 1. Specifically, an MOCO problem is decomposed into N single-objective subproblems with N weights, which are solved dependently by a unified heterogeneous graph attention (HGA) model θ . For each subproblem i , its features together with the current Pareto front \mathcal{F} (*points* in the objective space) constituted by preceding solutions are input to model θ , which is guided by the scalar objective with the HV indicator. Then, MPO is utilized to sample multiple solutions and efficiently update \mathcal{F} .

4.1 Indicator-enhanced DRL

Given a problem instance s , we sequentially solve its subproblem $i \in \{1, \dots, N\}$, each associated with weight λ^i . Let $\pi^i = \{\pi_1^i, \dots, \pi_T^i\}$ denote the obtained solution² at step i , and let \mathcal{F}^i be the Pareto front yielded by solutions from subproblem 1 to i . In each step i , we select up to K top *points* $\mathbf{f}(\pi) \in \mathcal{F}^{i-1}$ from the Pareto front at step $i-1$ with the ranking determined by the scalar objective $g(\pi|s, \lambda^i)$ with respect to the new given weight λ^i . The corresponding scalar objective and the induced surrogate landscape $\tilde{\mathcal{F}}^{i-1} \subseteq \mathcal{F}^{i-1}$ based on those selected solutions are treated as the policy network inputs (see Figure 2), so as to construct a new solution π^i and yield a new \mathcal{F}^i .

The construction of the solution π^i with length T for each subproblem i can be cast as a Markov decision process. In particular, 1) the *state* includes the weight λ^i , user-defined diversity factor $\mathbf{w}^i \in \mathcal{R}^2$ satisfying $w_1^i, w_2^i \geq 0$ and $w_1^i + w_2^i = 1$, partial solution $\pi_{1:t-1}^i$, instance s , and $\tilde{\mathcal{F}}_r^{i-1}$, where $\tilde{\mathcal{F}}_r^{i-1} = \tilde{\mathcal{F}}^{i-1} \cup \{\mathbf{r}\}$ incorporates the aforementioned surrogate landscape at step i and the given reference point \mathbf{r} ; 2) the *action* is to add a node π_t^i into $\pi_{1:t-1}^i$; 3) the *state transition* transforms $\pi_{1:t-1}^i$ to $\pi_{1:t}^i$, denoted as $\pi_{1:t}^i = \{\pi_{1:t-1}^i, \pi_t^i\}$; 4) the *reward* is defined as $R^i = -w_1^i \times g(\pi^i|s, \lambda^i) + w_2^i \times \text{HV}_r(\tilde{\mathcal{F}}^{i-1} \cup \{\mathbf{f}(\pi^i)\})$, where we introduce the hypervolume $\text{HV}_r(\tilde{\mathcal{F}}^{i-1} \cup \{\mathbf{f}(\pi^i)\})$ to guide the search; and 5) the stochastic *policy* generating the solution π^i is expressed as $P(\pi^i|s, \tilde{\mathcal{F}}_r^{i-1}, \lambda^i, \mathbf{w}^i) = \prod_{t=1}^T P_\theta(\pi_t^i|\pi_{1:t-1}^i, s, \tilde{\mathcal{F}}_r^{i-1}, \lambda^i, \mathbf{w}^i)$, with the probability of node selection $P_\theta(\pi_t^i|\pi_{1:t-1}^i, s, \tilde{\mathcal{F}}_r^{i-1}, \lambda^i, \mathbf{w}^i)$ parameterized by a deep model θ .

We would like to note that our NHDE is generic, and can directly integrate the base model θ with the existing decomposition-based neural MOCO methods. We demonstrate this property by applying it to two state-of-the-art methods, PMOCO [14] and MDRL [15], denoted as NHDE-P and NHDE-M, respectively. Given λ^i and \mathbf{w}^i as inputs, NHDE-P uses a hypernetwork to generate the decoder parameters of the model $\theta(\lambda^i, \mathbf{w}^i)$, while NHDE-M fine-tunes the pre-trained meta model θ_{meta} with a few steps to address the corresponding subproblem. More details are presented in Appendix B.

4.2 Heterogeneous graph attention

To effectively solve subproblem i , the model should jointly capture the representations of both the instance’s node graph and the Pareto front’s *point* graph. Based on the encoder-decoder structure, we thus design a heterogeneous graph attention (HGA) model to correlate the two heterogeneous graphs as depicted in Figure 2. In the following section, we omit superscript i for better readability.

Encoder. Given an instance graph s containing n nodes with Z -dimensional features and a Pareto front graph $\tilde{\mathcal{F}}_r^{i-1}$ containing k *points* ($k \leq K + 1$) with M -dimensional features, their initial embeddings $\mathbf{h}_1^{(0)}, \dots, \mathbf{h}_n^{(0)} \in R^d$ and $\mathbf{g}_1^{(0)}, \dots, \mathbf{g}_k^{(0)} \in R^d$ are yielded by a linear projection with trainable parameters W_h and W_g , respectively, and d is empirically set to 128. The eventual embeddings $\mathbf{h}_1^{(L)}, \dots, \mathbf{h}_n^{(L)}$ and $\mathbf{g}_1^{(L)}, \dots, \mathbf{g}_k^{(L)}$ are derived by further passing through $L = 6$ attention layers.

²In this sub-section, we consider the construction of only one solution in each step for better readability; however, we note that multiple solutions can be sampled and our formulation would work in a similar manner.

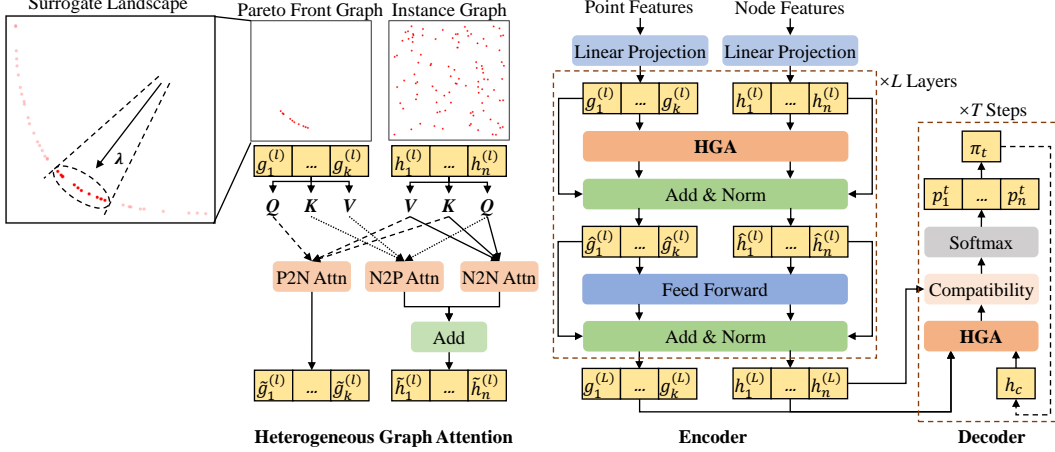


Figure 2: Illustration of the proposed heterogeneous graph attention (HGA) model.

Each attention layer is composed of a multi-head HGA layer with $Y = 8$ heads and a fully connected feed-forward sublayer. For layer $l \in \{1, \dots, L\}$, HGA computes the representations $\tilde{\mathbf{h}}_u^{(l)}$ and $\tilde{\mathbf{g}}_u^{(l)}$ across the heterogeneous graphs, which are used to update the embeddings $\mathbf{h}_u^{(l)}$ and $\mathbf{g}_u^{(l)}$. Skip-connection [49] and batch normalization [50] are both adopted in each sublayer, as follows,

$$\mathbf{h}_u^{(l)} = \text{BN}(\hat{\mathbf{h}}_u + \text{FF}(\hat{\mathbf{h}}_u)), \quad \hat{\mathbf{h}}_u = \text{BN}(\mathbf{h}_u^{(l-1)} + \tilde{\mathbf{h}}_u^{(l)}), \quad \forall u \in \{1, \dots, n\}, \quad (3)$$

$$\mathbf{g}_u^{(l)} = \text{BN}(\hat{\mathbf{g}}_u + \text{FF}(\hat{\mathbf{g}}_u)), \quad \hat{\mathbf{g}}_u = \text{BN}(\mathbf{g}_u^{(l-1)} + \tilde{\mathbf{g}}_u^{(l)}), \quad \forall u \in \{1, \dots, k\}. \quad (4)$$

Decoder. The decoder, composed of a multi-head HGA layer and a *compatibility* layer, autoregressively constructs a solution according to the probability distribution with T steps. At decoding step $t \in \{1, \dots, T\}$, the *glimpse* \mathbf{q}_c of the *context* embedding \mathbf{h}_c (see Appendix C) is computed by the HGA layer. Then, the *compatibility* α is calculated as follows,

$$\alpha_u = \begin{cases} -\infty, & \text{node } u \text{ is masked} \\ C \cdot \tanh\left(\frac{\mathbf{q}_c^T (W^K \mathbf{h}_u^{(L)})}{\sqrt{d/Y}}\right), & \text{otherwise} \end{cases} \quad (5)$$

where C is set to 10 [27]. Finally, softmax is employed to calculate the selection probability distribution $P_\theta(\pi|s, \tilde{\mathcal{F}}_r^{i-1}, \lambda^i, \mathbf{w}^i)$ for nodes, i.e., $P_\theta(\pi_t|\pi_{1:t-1}, s, \tilde{\mathcal{F}}_r^{i-1}, \lambda^i, \mathbf{w}^i) = \text{Softmax}(\alpha)$.

HGA. The HGA layer in the encoder captures three key relations between the node graph and the *point* graph. The first, *node-to-node* α_{uv}^{hh} , indicates each node's attention towards others within the same instance to construct a promising solution. The second, *node-to-point* α_{uv}^{hg} , suggests each node's attention to *points*, guiding the constructed solutions distinct from the existing ones in the current Pareto front. The third, *point-to-node* α_{uv}^{gh} , indicates each *point*'s attention to nodes, facilitating the learning of the mapping from a solution to its objective values. We disregard the less meaningful *point-to-point* attention. Concretely, Eq. (6) defines the above three attention scores, which are separately normalized as $\tilde{\alpha}_{uv}^{hh}$, $\tilde{\alpha}_{uv}^{hg}$, and $\tilde{\alpha}_{uv}^{gh}$ by softmax. Then, $\tilde{\mathbf{h}}_u$ and $\tilde{\mathbf{g}}_u$ are computed by Eq. (7).

$$\alpha_{uv}^{hh} = \frac{(W_h^Q \mathbf{h}_u)^T (W_h^K \mathbf{h}_v)}{\sqrt{d/Y}}, \quad \alpha_{uv}^{hg} = \frac{(W_h^Q \mathbf{h}_u)^T (W_g^K \mathbf{g}_v)}{\sqrt{d/Y}}, \quad \alpha_{uv}^{gh} = \frac{(W_g^Q \mathbf{g}_u)^T (W_h^K \mathbf{h}_v)}{\sqrt{d/Y}}. \quad (6)$$

$$\tilde{\mathbf{h}}_u = \sum_{v=1}^n \tilde{\alpha}_{uv}^{hh} W_h^V \mathbf{h}_v + \sum_{v=1}^k \tilde{\alpha}_{uv}^{hg} W_g^V \mathbf{g}_v, \quad \tilde{\mathbf{g}}_u = \sum_{v=1}^n \tilde{\alpha}_{uv}^{gh} W_h^V \mathbf{h}_v. \quad (7)$$

Finally, as for the multi-head attention, $\tilde{\mathbf{h}}_u$ and $\tilde{\mathbf{g}}_u$ are further computed as follows,

$$\tilde{\mathbf{h}}_u = W_h^O \text{Concat}(\tilde{\mathbf{h}}_{u,1}, \dots, \tilde{\mathbf{h}}_{u,Y}), \quad \tilde{\mathbf{g}}_u = W_g^O \text{Concat}(\tilde{\mathbf{g}}_{u,1}, \dots, \tilde{\mathbf{g}}_{u,Y}), \quad (8)$$

where $\tilde{\mathbf{h}}_{u,y}$ and $\tilde{\mathbf{g}}_{u,y}$ for head $y \in \{1, \dots, Y\}$ are obtained according to Eq. (7). In the multi-head HGA, W_h^Q , W_h^K , W_h^V , W_h^O , W_g^Q , W_g^K , W_g^V , and W_g^O are independent trainable parameters. Similarly, in the decoder, the *glimpse* \mathbf{q}_c is calculated by the *context* embedding \mathbf{h}_c with the addition of the *context-to-node* and *context-to-point* attention, i.e., replacing \mathbf{h}_u with \mathbf{h}_c in the Eq. (6–8).

Algorithm 1 Training algorithm of NHDE-P

```
1: Input: weight distribution  $\Lambda$ , diversity-factor distribution  $\mathcal{W}$ , instance distribution  $\mathcal{S}$ , number of
   training steps  $E$ , number of sampled weights per step  $N'$ , batch size  $B$ , instance size  $n$ 
2: Initialize the model parameters  $\theta$ 
3: for  $e = 1$  to  $E$  do
4:    $s_i \sim \text{SampleInstance}(\mathcal{S}) \quad \forall i \in \{1, \dots, B\}$ 
5:   Initialize  $\tilde{\mathcal{F}}_i \leftarrow \emptyset \quad \forall i$ 
6:   for  $n' = 1$  to  $N'$  do
7:      $\lambda \sim \text{SampleWeight}(\Lambda)$ 
8:      $w \sim \text{SampleDiversityFactor}(\mathcal{W})$ 
9:      $\pi_i^j \sim \text{SampleSolution}(P_{\theta(\lambda, w)}(\cdot | s_i, \tilde{\mathcal{F}}_{r,i}, \lambda, w)) \quad \forall i \in \{1, \dots, B\} \quad \forall j \in \{1, \dots, n\}$ 
10:     $R_i^j \leftarrow -w_1 g(\pi_i^j | s_i, \lambda) + w_2 \text{HV}_r(\tilde{\mathcal{F}}_i \cup \{\mathbf{f}(\pi_i^j)\}) \quad \forall i, j$ 
11:     $b_i \leftarrow \frac{1}{n} \sum_{j=1}^n (-R_i^j) \quad \forall i$ 
12:     $\nabla \mathcal{J}(\theta) \leftarrow \frac{1}{Bn} \sum_{i=1}^B \sum_{j=1}^n [(-R_i^j - b_i) \nabla_{\theta(\lambda, w)} \log P_{\theta(\lambda, w)}(\pi_i^j | s_i, \tilde{\mathcal{F}}_{r,i}, \lambda, w)]$ 
13:     $\theta \leftarrow \text{Adam}(\theta, \nabla \mathcal{J}(\theta))$ 
14:     $\mathcal{G}_i \leftarrow \{\mathbf{f}(\pi_i^1), \dots, \mathbf{f}(\pi_i^n)\} \quad \forall i$ 
15:     $\tilde{\mathcal{F}}_i \leftarrow \text{MPO}(\tilde{\mathcal{F}}_i \cup \mathcal{G}_i) \quad \forall i$ 
16:   end for
17: end for
18: Output: The model parameter  $\theta$ 
```

4.3 Multiple Pareto optima strategy

Contrary to single-objective problems that focus on a single optimal solution, MOCO problems involve a series of Pareto-optimal solutions. In light of this, we introduce a multiple Pareto optima (MPO) strategy to uncover multiple solutions for each subproblem by leveraging the Pareto optimality.

When solving subproblem i , more than one solution can be attained by sampling, e.g., sampling with multiple start nodes as did in POMO [36]. In this case, $\mathcal{F}^i = \text{MPO}(\mathcal{F}^{i-1} \cup \mathcal{G}^i)$, where \mathcal{G}^i contains all the candidate *points* (find by sampling) to be introduced in the new Pareto front and $\text{MPO}(\cdot)$ is an operator that updates the Pareto front. However, as the complexity of $\text{MPO}(\mathcal{F}^{i-1} \cup \mathcal{G}^i)$ is $O((|\mathcal{F}^{i-1}| + |\mathcal{G}^i|)|\mathcal{G}^i|)$, it may take a relatively long time, especially when there are thousands of *points* in \mathcal{F}^{i-1} and \mathcal{G}^i . Thus, we suggest an efficient update mechanism executed on the surrogate Pareto fronts, $\tilde{\mathcal{F}}^i = \text{MPO}(\tilde{\mathcal{F}}^{i-1} \cup \tilde{\mathcal{G}}^i)$, where $\tilde{\mathcal{G}}^i \subset \mathcal{G}^i$ includes at most J (usually setting $J > K$) best *points* selected from $\mathbf{f}(\pi) \in \mathcal{G}^i$ according to $g(\pi | s, \lambda^i)$. The complexity of $\text{MPO}(\tilde{\mathcal{F}}^{i-1} \cup \tilde{\mathcal{G}}^i)$ is then reduced to $O((K + J)J)$, which is able to curtail the overall solving time in practice.

4.4 Training and inference

Our NHDE can be applied to different decomposition-based DRL methods, e.g., PMOCO [14] and MDRL [15], and the training algorithm is easy to adapt with slight adjustments, where the one for NHDE-P is presented in Algorithm 1. The key points include three aspects. (1) Multiple weights are sampled to train the same instance (Line 6), since the solving processes for those subproblems are dependent. (2) The HV indicator is adopted in the reward (Line 10). (3) Multiple Pareto-optimal solutions are preserved via MPO (Line 15). Note that when training with a batch, the *point* sets with different sizes of the instances are padded with repetitive reference points, which are masked in the attention, based on the maximum size. The training algorithm of NHDE-M is given in Appendix E.

In the inference phase, for N given weights and diversity factors, the well-trained model is used to sequentially solve N corresponding subproblems, as shown in Figure 1. Moreover, instance augmentation [14] can be also brought into our MPO for each subproblem, i.e., the *points* of all sampled solutions from an instance and its augmented instances are included in \mathcal{G}^i . Our NHDE can achieve desirable performance by using only parts of instance augmentation (see Appendix D), since it can already deliver more diverse solutions.

5 Experiments

Problems. We evaluate the proposed NHDE on three typical MOCO problems that are commonly studied in the neural MOCO literature [13–15], namely the multi-objective traveling salesman problem (MOTSP) [51], multi-objective capacitated vehicle routing problem (MOCVRP) [3], and multi-objective knapsack problem (MOKP) [52]. More specifically, we solve bi-objective TSP (Bi-TSP), tri-objective TSP (Tri-TSP), the bi-objective CVRP (Bi-CVRP) and the bi-objective KP (Bi-KP). For the M -objective TSP with n nodes, each node has M sets of 2-dimensional coordinates, where the m -th objective value of the solution is calculated with respect to the m -th coordinates. Bi-CVRP consists of n customer nodes and a depot node, with each node featured by a 2-dimensional coordinate and each customer node associated with a demand. Following the literature, we consider two conflicting objectives in Bi-CVRP, i.e., the total tour length and the makespan (that is the length of the longest route). Bi-KP is defined by n items, with each taking a weight and two separate values. The m -th objective is to maximize the sum of the m -th values but not exceed the capacity. Three sizes of these problems are considered, i.e., $n=20/50/100$ for MOTSP and MOCVRP, and $n=50/100/200$ for MOKP. The coordinates, demands, and values are uniformly sampled from $[0, 1]^2$, $\{1, \dots, 9\}$, and $[0, 1]$, respectively. The vehicle capacity is set to 30/40/50 for MOCVRP20/50/100. The knapsack capacity is set to 12.5/25/25 for MOKP50/100/200.

Hyperparameters. We train NHDE-P with 200 epochs, each containing 5,000 randomly generated instances. We use batch size $B = 64$ and the Adam [53] optimizer with learning rate 10^{-4} (10^{-5} for MOKP) and weight decay 10^{-6} . During training, $N' = 20$ weights are sampled for each instance. During inference, we generate $N = 40$ and $N = 210$ uniformly distributed weights for $M = 2$ and $M = 3$, respectively, which are then shuffled so as to counteract biases. The diversity factors linearly shift through the N subproblems from (1,0) to (0,1), which implies a gradual focus from achieving convergence (scalar objective) with a few solutions to ensuring comprehensive performance with a multitude of solutions. We set $K = 20$ and $J = 200$. See Appendix F for the settings of NHDE-M.

Baselines. We compare NHDE with two classes of state-of-the-art methods. (1) The neural methods, including PMOCO [14], MDRL [15], and DRL-based multiobjective optimization algorithm (DRL-MOA) [13], all with POMO as the backbone for single-objective CO subproblems. Our NHDE-P and NHDE-M each train a unified model with the same gradient steps as PMOCO and MDRL, respectively, while DRL-MOA trains 101 (105) models for $M = 2$ ($M = 3$) with more gradient steps, i.e., the first model with 200 epochs and the remaining models with 5-epoch per model via parameter transfer. (2) The non-learnable methods, including the state-of-the-art MOEA and strong heuristics. Particularly, PPLS/D-C [23] is a specialized MOEA for MOCO with local search techniques, including a 2-opt heuristic for MOTSP and MOCVRP, and a greedy transformation heuristic [52] for MOKP, implemented in Python. In addition, LKH [54, 55] and dynamic programming (DP), are employed to solve the weighted-sum (WS) based subproblems for MOTSP and MOKP, denoted as **WS-LKH** and **WS-DP**, respectively. All the methods use WS scalarization for fair comparisons. All the methods are tested with an RTX 3090 GPU and an Intel Xeon 4216 CPU. Our code is publicly available³.

Metrics. We use hypervolume (HV) and the number of non-dominated solutions ($|\text{NDS}|$). A higher HV means better overall performance in terms of convergence and diversity, while $|\text{NDS}|$ reflects the diversity when HVs are close. The average HV, gaps with respect to NHDE, and total running time for 200 random test instances are reported. The best (second-best) and its statistically insignificant results at 1% significance level of a Wilcoxon rank-sum test are highlighted in **bold** (underline).

5.1 Main results

All results of NHDE-P and the baselines are displayed in Table 1. Given the same number of weights (wt.), NHDE-P significantly surpasses PMOCO for all problems and sizes in terms of HV and $|\text{NDS}|$, which indicates that NHDE-P has the potential to discover diverse and high-quality solutions. When instance augmentation (aug.) is equipped, NHDE-P achieves the smallest gap among the methods in most cases, except Bi-TSP100 and Bi-CVRP100 where WS-LKH and DRL-MOA perform better. However, WS-LKH consumes much longer runtime than NHDE-P due to iterative search (2.7 hours vs 5.6 minutes), and DRL-MOA costs much more training overhead to prepare multiple models for respective weights. Besides, another reason why NHDE-P is inferior to DRL-MOA on Bi-CVRP100 might be that the hypernetwork (inherited from PMOCO) could be hard to cope with the objectives

³<https://github.com/bill-cjb/NHDE>

Table 1: Results of NHDE-P on 200 random instances for MOCO problems.

Method	Bi-TSP20				Bi-TSP50				Bi-TSP100			
	HV↑	NDS ↑	Gap↓	Time	HV↑	NDS ↑	Gap↓	Time	HV↑	NDS ↑	Gap↓	Time
WS-LKH (40 wt.)	0.6266	14	0.46%	4.1m	0.6402	29	0.42%	42m	0.7072	37	-0.31%	2.7h
PPLS/D-C (200 iter.)	0.6256	71	0.62%	26m	0.6282	213	2.29%	2.8h	0.6844	373	2.92%	11h
DRL-MOA (101 models)	0.6257	23	0.60%	6s	0.6360	57	1.07%	9s	0.6970	70	1.13%	21s
PMOCO (40 wt.)	0.6258	17	0.59%	4s	0.6331	31	1.52%	5s	0.6938	36	1.59%	8s
PMOCO (600 wt.)	0.6267	23	0.44%	27s	0.6361	68	1.06%	53s	0.6978	131	1.02%	2.1m
NHDE-P (40 wt.)	<u>0.6286</u>	56	<u>0.14%</u>	19s	0.6388	127	0.64%	53s	0.7005	193	0.64%	1.9m
PMOCO (40 wt. aug.)	0.6266	17	0.46%	23s	0.6377	32	0.81%	1.6m	0.6993	37	0.81%	3.0m
PMOCO (100 wt. aug.)	0.6270	20	0.40%	1.4m	0.6395	53	0.53%	3.8m	0.7016	76	0.48%	15m
NHDE-P (40 wt. aug.)	0.6295	81	0.00%	1.5m	0.6429	269	0.00%	2.5m	<u>0.7050</u>	343	<u>0.00%</u>	5.6m
Method	Bi-CVRP20				Bi-CVRP50				Bi-CVRP100			
	HV↑	NDS ↑	Gap↓	Time	HV↑	NDS ↑	Gap↓	Time	HV↑	NDS ↑	Gap↓	Time
PPLS/D-C (200 iter.)	0.4283	14	0.46%	1.3h	0.4007	17	2.15%	9.7h	0.3946	20	1.13%	38h
DRL-MOA (101 models)	0.4287	7	0.37%	10s	0.4076	10	0.46%	12s	0.4055	12	-1.60%	33s
PMOCO (40 wt.)	0.4266	6	0.86%	4s	0.4035	7	1.47%	7s	0.3912	6	1.98%	12s
PMOCO (300 wt.)	0.4268	7	0.81%	20s	0.4039	9	1.37%	35s	0.3914	8	1.93%	1.2m
NHDE-P (40 wt.)	0.4284	12	0.44%	18s	0.4062	14	0.81%	36s	0.3933	10	1.45%	1.1m
PMOCO (40 wt. aug.)	0.4292	6	0.26%	8s	0.4078	7	0.42%	15s	0.3968	7	0.58%	1.1m
PMOCO (300 wt. aug.)	<u>0.4294</u>	9	<u>0.21%</u>	1.0m	0.4081	10	0.34%	1.8m	0.3969	9	0.55%	7.0m
NHDE-P (40 wt. aug.)	0.4303	21	0.00%	1.2m	0.4095	22	0.00%	1.5m	<u>0.3991</u>	16	<u>0.00%</u>	2.4m
Method	Bi-KP50				Bi-KP100				Bi-KP200			
	HV↑	NDS ↑	Gap↓	Time	HV↑	NDS ↑	Gap↓	Time	HV↑	NDS ↑	Gap↓	Time
WS-DP (40 wt.)	<u>0.3560</u>	10	<u>0.11%</u>	9.6m	0.4529	16	0.26%	1.3h	0.3598	23	0.39%	3.8h
PPLS/D-C (200 iter.)	0.3528	13	1.01%	18m	0.4480	19	1.34%	47m	0.3541	20	1.97%	1.5h
DRL-MOA (101 models)	0.3559	21	0.14%	9s	<u>0.4531</u>	38	<u>0.22%</u>	18s	<u>0.3601</u>	48	<u>0.30%</u>	1.0m
PMOCO (40 wt.)	0.3550	14	0.39%	6s	0.4518	22	0.51%	9s	0.3590	28	0.61%	25s
PMOCO (300 wt.)	0.3552	17	0.34%	29s	0.4524	31	0.37%	1.1m	0.3597	46	0.42%	3.0m
NHDE-P (40 wt.)	0.3564	30	0.00%	29s	0.4541	83	0.00%	1.0m	0.3612	243	0.00%	2.7m
Method	Tri-TSP20				Tri-TSP50				Tri-TSP100			
	HV↑	NDS ↑	Gap↓	Time	HV↑	NDS ↑	Gap↓	Time	HV↑	NDS ↑	Gap↓	Time
WS-LKH (210 wt.)	0.4727	78	0.82%	23m	0.4501	189	1.90%	3.5h	<u>0.5165</u>	209	<u>0.84%</u>	12h
PPLS/D-C (200 iter.)	0.4698	876	1.43%	1.4h	0.4174	3727	9.02%	3.9h	0.4376	8105	15.99%	14h
DRL-MOA (105 models)	0.4675	72	1.91%	5s	0.4285	98	6.61%	9s	0.4850	101	6.89%	19s
PMOCO (210 wt.)	0.4714	113	1.09%	11s	0.4381	198	4.51%	18s	0.4946	207	5.05%	39s
PMOCO (3003 wt.)	0.4741	264	0.52%	2.3m	0.4484	1339	2.27%	4.6m	0.5087	2330	2.34%	10m
NHDE-P (210 wt.)	<u>0.4758</u>	675	<u>0.17%</u>	1.2m	<u>0.4506</u>	2547	<u>1.79%</u>	4.4m	0.5111	4984	1.88%	10m
PMOCO (210 wt. aug.)	0.4727	104	0.82%	21m	0.4471	201	2.55%	1.1h	0.5044	209	3.17%	4.2h
PMOCO (153 wt. aug.)	0.4722	89	0.92%	15m	0.4447	150	3.07%	47m	0.5009	153	3.84%	3.1h
NHDE-P (210 wt. aug.)	0.4766	527	0.00%	14m	0.4588	9047	0.00%	30m	0.5209	16999	0.00%	1.5h

with imbalanced scales. Considering this drawback of PMOCO, we also apply our method to MDRL, i.e., NHDE-M, and demonstrate that NHDE-M outperforms DRL-MOA on Bi-CVRP100 in Table 2. Also, NHDE-M outperforms MDRL in all cases. More results of NHDE-M are given in Appendix G.

Regarding the inference efficiency, NHDE-P generally takes (tolerably) more runtime than the other learning based methods. To be fair, we further enhance the state-of-the-art PMOCO by adjusting the number of the weights, so that it takes similar or even more runtime compared with NHDE-P. The results in the last two lines for each problem shows that NHDE-P still attains the smaller gaps. We also observe that |NDS| hardly grows along with the increase of number of weights for PMOCO, since numerous solutions to different subproblems could be repetitive. In contrast, NHDE-P is able to produce more diverse solutions with much fewer weights.

5.2 Generalization study

To assess the generalization capability of NHDE-P, we compare the trained models (from neural methods) for Bi-TSP100 and the other baselines on 200 random Bi-TSP instances with larger sizes, i.e., Bi-TSP150/200. Three commonly used benchmark instances developed from TSPLIB [56],

Table 2: Results of NHDE-M on 200 random instances for MOCO problems.

Method	Bi-TSP20				Bi-TSP50				Bi-TSP100			
	HV↑	NDS ↑	Gap↓	Time	HV↑	NDS ↑	Gap↓	Time	HV↑	NDS ↑	Gap↓	Time
WS-LKH (40 wt.)	0.6266	14	0.46%	4.1m	0.6402	29	0.42%	42m	0.7072	37	-0.33%	2.7h
PPLS/D-C (200 iter.)	0.6256	71	0.62%	26m	0.6282	213	2.29%	2.8h	0.6844	373	2.91%	11h
DRL-MOA (101 models)	0.6257	23	0.60%	6s	0.6360	57	1.07%	9s	0.6970	70	1.12%	21s
MDRL (40 wt.)	0.6264	20	0.49%	2s	0.6342	33	1.35%	3s	0.6940	36	1.55%	8s
NHDE-M (40 wt.)	<u>0.6287</u>	58	<u>0.13%</u>	20s	0.6393	132	0.56%	57s	0.7008	195	0.58%	2.0m
MDRL (40 wt. aug.)	0.6267	18	0.44%	21s	0.6384	34	0.70%	1.5m	0.6995	38	0.77%	3.3m
NHDE-M (40 wt. aug.)	0.6295	81	0.00%	1.5m	0.6429	273	0.00%	2.6m	<u>0.7049</u>	339	<u>0.00%</u>	5.5m
Method	Bi-CVRP20				Bi-CVRP50				Bi-CVRP100			
	HV↑	NDS ↑	Gap↓	Time	HV↑	NDS ↑	Gap↓	Time	HV↑	NDS ↑	Gap↓	Time
PPLS/D-C (200 iter.)	0.4287	15	0.42%	1.6h	0.4007	17	2.34%	9.7h	0.3946	20	3.14%	38h
DRL-MOA (101 models)	0.4287	7	0.42%	10s	0.4076	10	0.66%	12s	<u>0.4055</u>	12	<u>0.47%</u>	33s
MDRL (40 wt.)	0.4284	9	0.49%	3s	0.4057	5	1.12%	5s	0.4015	0	1.45%	10s
NHDE-M (40 wt.)	<u>0.4296</u>	16	<u>0.21%</u>	23s	<u>0.4086</u>	20	<u>0.41%</u>	47s	0.4053	18	0.52%	1.4m
MDRL (40 wt. aug.)	0.4293	9	0.28%	5s	0.4073	11	0.73%	16s	0.4040	11	0.83%	1.0m
NHDE-M (40 wt. aug.)	0.4305	24	0.00%	1.2m	0.4103	29	0.00%	1.6m	0.4074	26	0.00%	2.7m
Method	Bi-KP50				Bi-KP100				Bi-KP200			
	HV↑	NDS ↑	Gap↓	Time	HV↑	NDS ↑	Gap↓	Time	HV↑	NDS ↑	Gap↓	Time
WS-DP (40 wt.)	<u>0.3560</u>	10	<u>0.17%</u>	9.6m	0.4529	16	0.29%	1.3h	0.3598	23	0.30%	3.8h
PPLS/D-C (200 iter.)	0.3528	13	1.07%	18m	0.4480	19	1.37%	47m	0.3541	20	1.88%	1.5h
DRL-MOA (101 models)	0.3559	21	0.20%	9s	<u>0.4531</u>	38	<u>0.24%</u>	18s	<u>0.3601</u>	48	<u>0.22%</u>	1.0m
MDRL (40 wt.)	0.3559	17	0.20%	4s	0.4528	25	0.31%	8s	0.3594	31	0.42%	24s
NHDE-M (40 wt.)	0.3566	41	0.00%	31s	0.4542	93	0.00%	1.0m	0.3609	160	0.00%	2.8m
Method	Tri-TSP20				Tri-TSP50				Tri-TSP100			
	HV↑	NDS ↑	Gap↓	Time	HV↑	NDS ↑	Gap↓	Time	HV↑	NDS ↑	Gap↓	Time
WS-LKH (210 wt.)	0.4727	78	0.82%	23m	0.4501	189	2.00%	3.5h	0.5165	209	-0.92%	12h
PPLS/D-C (200 iter.)	0.4698	876	1.43%	1.4h	0.4174	3727	9.12%	3.9h	0.4376	8105	14.50%	14h
DRL-MOA (105 models)	0.4675	72	1.91%	5s	0.4285	98	6.71%	9s	0.4850	101	5.24%	19s
MDRL (210 wt.)	0.4723	126	0.90%	14s	0.4388	199	4.46%	20s	0.4956	207	3.17%	40s
NHDE-M (210 wt.)	<u>0.4763</u>	783	<u>0.06%</u>	1.4m	<u>0.4512</u>	2636	<u>1.76%</u>	4.7m	0.4997	4056	2.36%	11m
MDRL (210 wt. aug.)	0.4727	107	0.82%	14m	0.4473	202	2.61%	53m	0.5056	209	1.21%	4.3h
NHDE-M (210 wt. aug.)	0.4766	748	0.00%	13m	0.4593	10850	0.00%	30m	<u>0.5118</u>	13216	<u>0.00%</u>	1.5h

Table 3: Results on 200 random instances for larger-scale problems.

Method	Bi-TSP150				Bi-TSP200			
	HV↑	NDS ↑	Gap↓	Time	HV↑	NDS ↑	Gap↓	Time
WS-LKH (40 wt.)	0.7075	39	-0.90%	5.3h	0.7435	40	-1.52%	8.5h
PPLS/D-C (200 iter.)	0.6784	473	3.25%	21h	0.7106	512	2.98%	32h
DRL-MOA (101 models)	0.6901	73	1.58%	45s	0.7219	75	1.43%	87s
PMOCO (40 wt.)	0.6891	37	1.73%	22s	0.7215	38	1.49%	41s
PMOCO (400 wt.)	0.6938	160	1.06%	3.7m	0.7259	186	0.89%	6.8m
NHDE-P (40 wt.)	0.6964	231	0.68%	3.0m	0.7280	259	0.60%	4.3m
PMOCO (40 wt. aug.)	0.6944	38	0.97%	20m	0.7264	39	0.82%	40m
NHDE-P (40 wt. aug.)	<u>0.7012</u>	372	<u>0.00%</u>	14m	<u>0.7324</u>	384	<u>0.00%</u>	26m

i.e., KroAB100, KroAB150, and KroAB200, are also tested. The comparison results and Pareto fronts are demonstrated in Table 3 and Figure 3, respectively. As shown, NHDE-P outperforms the state-of-the-art MOEA (i.e., PPLS/D-C) and other neural methods significantly, in terms of HV and |NDS|, which means a superior generalization capability. The figure again verifies that NHDE-P generates a more extended Pareto front than PMOCO, showing a better diversity. Although PPLS/D-C finds a large number of solutions, they are inferior in terms of the optimality, with a biased distribution (e.g., crowded in certain regions). In contrast, NHDE-P generates a more well-distributed Pareto front with stronger convergence. More results on generalization are given in Appendix H.

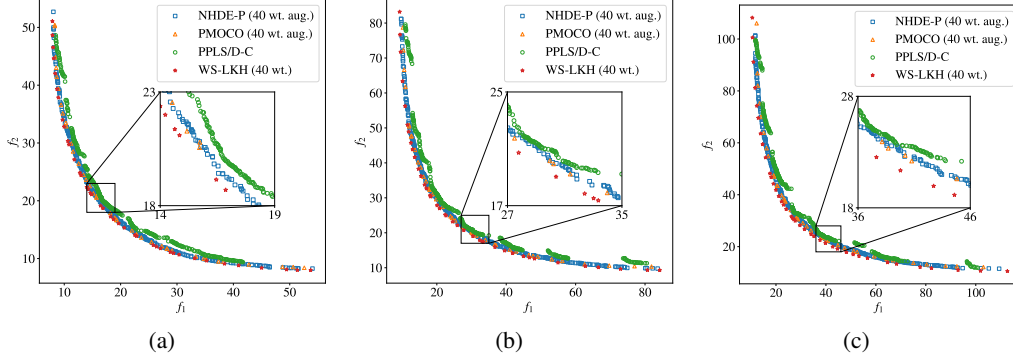


Figure 3: Pareto fronts of benchmark instances. (a) KroAB100. (b) KroAB150. (c) KroAB200.

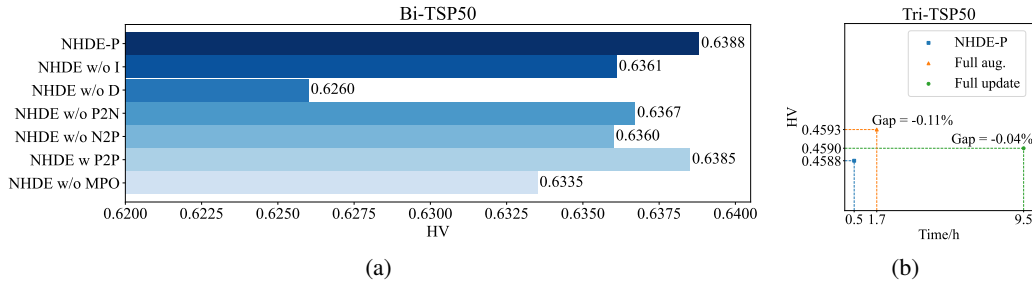


Figure 4: Ablation study. (a) Effects of indicator-enhanced DRL, HGA, and MPO. (b) Effects of the efficient update of MPO and partial instance augmentation.

5.3 Ablation Study

To analyze the effect of the indicator-enhanced DRL, we compare NHDE-P with decomposition-based DRL without indicator (NHDE w/o I) and indicator-based DRL without decomposition (NHDE w/o D). To verify the valid design of HGA, three attention-based variants, which are formed by removing *point-to-node* attention (NHDE w/o P2N), removing *node-to-point* attention (NHDE w/o N2P), and adding *point-to-point* attention (NHDE w P2P), are involved for comparison. To assess the impact of MPO, NHDE w/o MPO is also evaluated. More details about these variants are presented in Appendix I. As seen from Figure 4(a). The performance of NHDE-P is significantly impaired when any of the components is ablated. Instead, NHDE w P2P degrades a bit, which reveals that the extra *point-to-point* attention may bring noises into the model. Moreover, we evaluate the effectiveness of the efficient update of MPO and partial instance augmentation in Figure 4(b), which shows that either of them saliently diminishes solving time with only a little sacrifice of the performance.

6 Conclusion

This paper proposes a novel NHDE for MOCO problems. NHDE impedes repetitive solutions from different subproblems via indicator-enhanced DRL with a HGA model, and digs more solutions in the neighborhood of each subproblem with an MPO strategy. Our generic NHDE can be deployed to different neural MOCO methods. The experimental results on three classic MOCO problems showed the superiority of NHDE, especially with regard to the diversity of Pareto set. A limitation is that the HV calculation would expend additional computational time, which might hinder the scalability of NHDE for solving much larger problems with many objectives. In the future, we will explore alternative schemes like the HV approximations [57, 58] to further promote the training efficiency of NHDE, and we also intend to apply it to tackle real-world MOCO problems.

Acknowledgments and disclosure of funding

This work is supported by the National Natural Science Foundation of China (62072483), and the Guangdong Basic and Applied Basic Research Foundation (2022A1515011690, 2021A1515012298).

References

- [1] Naveen Saini and Sriparna Saha. Multi-objective optimization techniques: a survey of the state-of-the-art and applications: Multi-objective optimization techniques. *The European Physical Journal Special Topics*, 230(10):2319–2335, 2021.
- [2] Qi Liu, Xiaofeng Li, Haitao Liu, and Zhaoxia Guo. Multi-objective metaheuristics for discrete optimization problems: A review of the state-of-the-art. *Applied Soft Computing*, 93:106382, 2020.
- [3] Sandra Zajac and Sandra Huber. Objectives and methods in multi-objective routing problems: a survey and classification scheme. *European Journal of Operational Research*, 290(1):1–25, 2021.
- [4] Alper Türkyılmaz, Özlem Şenvar, İrem Ünal, and Serol Bulkan. A research survey: heuristic approaches for solving multi objective flexible job shop problems. *Journal of Intelligent Manufacturing*, 31:1949–1983, 2020.
- [5] Yunfei Cui, Zhiqiang Geng, Qunxiong Zhu, and Yongming Han. Multi-objective optimization methods and application in energy saving. *Energy*, 125:681–704, 2017.
- [6] Zesong Fei, Bin Li, Shaoshi Yang, Chengwen Xing, Hongbin Chen, and Lajos Hanzo. A survey of multi-objective optimization in wireless sensor networks: Metrics, algorithms, and open problems. *IEEE Communications Surveys & Tutorials*, 19(1):550–586, 2017.
- [7] Matthias Ehrgott, Xavier Gandibleux, and Anthony Przybylski. Exact methods for multi-objective combinatorial optimisation. *Multiple criteria decision analysis: State of the art surveys*, pages 817–850, 2016.
- [8] Arne Herzel, Stefan Ruzika, and Clemens Thielen. Approximation methods for multiobjective optimization problems: A survey. *INFORMS Journal on Computing*, 33(4):1284–1299, 2021.
- [9] Cong Zhang, Yaixin Wu, Yining Ma, Wen Song, Zhang Le, Zhiguang Cao, and Jie Zhang. A review on learning to solve combinatorial optimisation problems in manufacturing. *IET Collaborative Intelligent Manufacturing*, 5(1):e12072, 2023.
- [10] Nina Mazyavkina, Sergey Sviridov, Sergei Ivanov, and Evgeny Burnaev. Reinforcement learning for combinatorial optimization: A survey. *Computers & Operations Research*, 134:105400, 2021.
- [11] Yoshua Bengio, Andrea Lodi, and Antoine Prouvost. Machine learning for combinatorial optimization: a methodological tour d’horizon. *European Journal of Operational Research*, 290(2):405–421, 2021.
- [12] Yimo Yan, Andy HF Chow, Chin Pang Ho, Yong-Hong Kuo, Qihao Wu, and Chengshuo Ying. Reinforcement learning for logistics and supply chain management: Methodologies, state of the art, and future opportunities. *Transportation Research Part E: Logistics and Transportation Review*, 162:102712, 2022.
- [13] Kaiwen Li, Tao Zhang, and Rui Wang. Deep reinforcement learning for multiobjective optimization. *IEEE Transactions on Cybernetics*, 51(6):3103–3114, 2021.
- [14] Xi Lin, Zhiyuan Yang, and Qingfu Zhang. Pareto set learning for neural multi-objective combinatorial optimization. In *International Conference on Learning Representations*, 2022.
- [15] Zizhen Zhang, Zhiyuan Wu, Hang Zhang, and Jiahai Wang. Meta-learning-based deep reinforcement learning for multiobjective optimization problems. *IEEE Transactions on Neural Networks and Learning Systems*, 34(10):7978–7991, 2023.
- [16] Yaixin Wu, Wen Song, Zhiguang Cao, Jie Zhang, Abhishek Gupta, and Mingyan Lin. Graph learning assisted multi-objective integer programming. In *Advances in Neural Information Processing Systems*, 2022.
- [17] David Bergman, Merve Bodur, Carlos Cardonha, and Andre A Cire. Network models for multiobjective discrete optimization. *INFORMS Journal on Computing*, 34(2):990–1005, 2022.
- [18] Kalyanmoy Deb, Amrit Pratap, Sameer Agarwal, and TAMT Meyarivan. A fast and elitist multiobjective genetic algorithm: NSGA-II. *IEEE Transactions on Evolutionary Computation*, 6(2):182–197, 2002.

- [19] Qingfu Zhang and Hui Li. MOEA/D: A multiobjective evolutionary algorithm based on decomposition. *IEEE Transactions on Evolutionary Computation*, 11(6):712–731, 2007.
- [20] Nicola Beume, Boris Naujoks, and Michael Emmerich. Sms-emoa: Multiobjective selection based on dominated hypervolume. *European Journal of Operational Research*, 181(3):1653–1669, 2007.
- [21] Andrzej Jaszkievicz. Genetic local search for multi-objective combinatorial optimization. *European Journal of Operational Research*, 137(1):50–71, 2002.
- [22] Jialong Shi, Qingfu Zhang, and Jianyong Sun. PPLS/D: Parallel pareto local search based on decomposition. *IEEE transactions on cybernetics*, 50(3):1060–1071, 2020.
- [23] Jialong Shi, Jianyong Sun, Qingfu Zhang, Haotian Zhang, and Ye Fan. Improving pareto local search using cooperative parallelism strategies for multiobjective combinatorial optimization. *IEEE Transactions on Cybernetics*, 2022.
- [24] Oriol Vinyals, Meire Fortunato, and Navdeep Jaitly. Pointer networks. In *Advances in Neural Information Processing Systems*, 2015.
- [25] Irwan Bello, Hieu Pham, Quoc V Le, Mohammad Norouzi, and Samy Bengio. Neural combinatorial optimization with reinforcement learning. In *International Conference on Learning Representations*, 2017.
- [26] Mohammadreza Nazari, Afshin Oroojlooy, Martin Takáč, and Lawrence V. Snyder. Reinforcement learning for solving the vehicle routing problem. In *Advances in Neural Information Processing Systems*, 2018.
- [27] Wouter Kool, Herke Van Hoof, and Max Welling. Attention, learn to solve routing problems! In *International Conference on Learning Representations*, 2019.
- [28] Ashish Vaswani, Noam Shazeer, Niki Parmar, Jakob Uszkoreit, Llion Jones, Aidan N. Gomez, Łukasz Kaiser, and Illia Polosukhin. Attention is all you need. In *Advances in Neural Information Processing Systems*, 2017.
- [29] Liang Xin, Wen Song, Zhiguang Cao, and Jie Zhang. Multi-decoder attention model with embedding glimpse for solving vehicle routing problems. In *AAAI Conference on Artificial Intelligence*, pages 12042–12049, 2021.
- [30] Yeong-Dae Kwon, Jinho Choo, Iljoo Yoon, Minah Park, Duwon Park, and Youngjune Gwon. Matrix encoding networks for neural combinatorial optimization. In *Advances in Neural Information Processing Systems*, 2021.
- [31] Minsu Kim, Junyoung Park, and Jinkyoo Park. Sym-NCO: Leveraging symmetricity for neural combinatorial optimization. In *Advances in Neural Information Processing Systems*, 2022.
- [32] Jieyi Bi, Yining Ma, Jiahai Wang, Zhiguang Cao, Jinbiao Chen, Yuan Sun, and Yeow Meng Chee. Learning generalizable models for vehicle routing problems via knowledge distillation. In *Advances in Neural Information Processing Systems*, 2022.
- [33] Jinbiao Chen, Huanhuan Huang, Zizhen Zhang, and Jiahai Wang. Deep reinforcement learning with two-stage training strategy for practical electric vehicle routing problem with time windows. In *International Conference on Parallel Problem Solving from Nature*, 2022.
- [34] Zizhen Zhang, Hong Liu, MengChu Zhou, and Jiahai Wang. Solving dynamic traveling salesman problems with deep reinforcement learning. *IEEE Transactions on Neural Networks and Learning Systems*, 34(4): 2119–2132, 2023.
- [35] Jianan Zhou, Yaixin Wu, Wen Song, Zhiguang Cao, and Jie Zhang. Towards omni-generalizable neural methods for vehicle routing problems. In *the 40th International Conference on Machine Learning*, 2023.
- [36] Yeong-Dae Kwon, Jinho Choo, Byoungjip Kim, Iljoo Yoon, Youngjune Gwon, and Seungjai Min. POMO: Policy optimization with multiple optima for reinforcement learning. In *Advances in Neural Information Processing Systems*, 2020.
- [37] Xinyun Chen and Yuandong Tian. Learning to perform local rewriting for combinatorial optimization. In *Advances in Neural Information Processing Systems*, 2019.
- [38] Hao Lu, Xingwen Zhang, and Shuang Yang. A learning-based iterative method for solving vehicle routing problems. In *International Conference on Learning Representations*, 2020.

- [39] Yaoxin Wu, Wen Song, Zhiguang Cao, Jie Zhang, and Andrew Lim. Learning improvement heuristics for solving routing problems. *IEEE Transactions on Neural Networks and Learning Systems*, 33(9):5057–5069, 2022.
- [40] Yining Ma, Jingwen Li, Zhiguang Cao, Wen Song, Le Zhang, Zhenghua Chen, and Jing Tang. Learning to iteratively solve routing problems with dual-aspect collaborative transformer. In *Advances in Neural Information Processing Systems*, 2021.
- [41] Yining Ma, Jingwen Li, Zhiguang Cao, Wen Song, Hongliang Guo, Yuejiao Gong, and Yeow Meng Chee. Efficient neural neighborhood search for pickup and delivery problems. In *International Joint Conferences on Artificial Intelligence*, 2022.
- [42] Xi Lin, Zhiyuan Yang, Xiaoyuan Zhang, and Qingfu Zhang. Pareto set learning for expensive multi-objective optimization. In *Advances in Neural Information Processing Systems*, 2022.
- [43] Aviv Navon, Aviv Shamsian, Ethan Fetaya, and Gal Chechik. Learning the pareto front with hypernetworks. In *International Conference on Learning Representations*, 2021.
- [44] Xi Lin, Hui-Ling Zhen, Zhenhua Li, Qing-Fu Zhang, and Sam Kwong. Pareto multi-task learning. In *Advances in neural information processing systems*, 2019.
- [45] Hong Wu, Jiahai Wang, and Zizhen Zhang. MODRL/D-AM: Multiobjective deep reinforcement learning algorithm using decomposition and attention model for multiobjective optimization. In *ISICA 2019*, volume CCIS 1205, pages 575–589, 2020.
- [46] Yinan Shao, Jerry Chun-Wei Lin, Gautam Srivastava, Dongdong Guo, Hongchun Zhang, Hu Yi, and Alireza Jolfaei. Multi-objective neural evolutionary algorithm for combinatorial optimization problems. *IEEE Transactions on Neural Networks and Learning Systems*, 34(4):2133–2143, 2023.
- [47] Yongxin Zhang, Jiahai Wang, Zizhen Zhang, and Yalan Zhou. MODRL/D-EL: Multiobjective deep reinforcement learning with evolutionary learning for multiobjective optimization. In *International Joint Conference on Neural Networks*, 2021.
- [48] Charles Audet, Jean Bignon, Dominique Cartier, Sébastien Le Digabel, and Ludovic Salomon. Performance indicators in multiobjective optimization. *European Journal of Operational Research*, 292(2):397–422, 2021.
- [49] Kaiming He, Xiangyu Zhang, Shaoqing Ren, and Jian Sun. Deep residual learning for image recognition. In *IEEE Conference on Computer Vision and Pattern Recognition*, pages 770–778, 2016.
- [50] Sergey Ioffe and Christian Szegedy. Batch normalization: Accelerating deep network training by reducing internal covariate shift. In *International Conference on Machine Learning*, volume 37, pages 448–456, 2015.
- [51] Thibaut Lust and Jacques Teghem. The multiobjective traveling salesman problem: A survey and a new approach. In *Advances in Multi-Objective Nature Inspired Computing*, pages 119–141, 2010.
- [52] Hisao Ishibuchi, Naoya Akedo, and Yusuke Nojima. Behavior of multiobjective evolutionary algorithms on many-objective knapsack problems. *IEEE Transactions on Evolutionary Computation*, 19(2):264–283, 2015.
- [53] Diederik P Kingma and Jimmy Ba. Adam: A method for stochastic optimization. In *International Conference on Learning Representations*, 2015.
- [54] Keld Helsgaun. An effective implementation of the lin–kernighan traveling salesman heuristic. *European Journal of Operational Research*, 126(1):106–130, 2000.
- [55] Renato Tinós, Keld Helsgaun, and Darrell Whitley. Efficient recombination in the lin–kernighan–helsgaun traveling salesman heuristic. In *International Conference on Parallel Problem Solving from Nature*, pages 95–107, 2018.
- [56] Gerhard Reinelt. TSPLIB—a traveling salesman problem library. *ORSA Journal on Computing*, 3(4): 376–384, 1991.
- [57] Jim Boelrijk, Bernd Ensing, and Patrick Forré. Multi-objective optimization via equivariant deep hypervolume approximation. In *International Conference on Learning Representations*, 2023.
- [58] Ke Shang, Weiyu Chen, Weiduo Liao, and Hisao Ishibuchi. Hv-net: Hypervolume approximation based on deepsets. *IEEE Transactions on Evolutionary Computation*, 2022.

Neural Multi-Objective Combinatorial Optimization with Diversity Enhancement (Appendix)

A Reference point and hypervolume ratio

The normalized hypervolume (HV) ratio is calculated as $HV'_r(\mathcal{F}) = HV_r(\mathcal{F}) / \prod_{i=1}^M |r_i - z_i|$, where \mathbf{r} is a reference point satisfying $r_i > \max\{f_i(\mathbf{x}) | \mathbf{f}(\mathbf{x}) \in \mathcal{F}\}$ and \mathbf{z} is an ideal point satisfying $z_i < \min\{f_i(\mathbf{x}) | \mathbf{f}(\mathbf{x}) \in \mathcal{F}\}$ ⁴, $\forall i \in \{1, \dots, M\}$. The used \mathbf{r} and \mathbf{z} are given in Table 4.

Table 4: Reference points and ideal points

Problem	Size	\mathbf{r}	\mathbf{z}
Bi-TSP	20	(20, 20)	(0, 0)
	50	(35, 35)	(0, 0)
	100	(65, 65)	(0, 0)
	150	(85, 85)	(0, 0)
	200	(115, 115)	(0, 0)
Bi-CVRP	20	(30, 4)	(0, 0)
	50	(45, 4)	(0, 0)
	100	(80, 4)	(0, 0)
Bi-KP	50	(5, 5)	(30, 30)
	100	(20, 20)	(50, 50)
	200	(30, 30)	(75, 75)
Tri-TSP	20	(20, 20, 20)	(0, 0)
	50	(35, 35, 35)	(0, 0)
	100	(65, 65, 65)	(0, 0)

B Details of NHDE-P and NHDE-M

NHDE-P, deploying NHDE to PMOCO [14], employs a hypernetwork to tackle the weight λ and diversity factor \mathbf{w} for the corresponding subproblem. Specifically, according to the given λ and \mathbf{w} , the hypernetwork generates the decoder parameters of the heterogeneous graph attention (HGA) model θ , which is an encoder-decoder-styled architecture, i.e., $\theta(\lambda, \mathbf{w}) = [\theta_{\text{en}}, \theta_{\text{de}}(\lambda, \mathbf{w})]$, as shown in Figure 5. Following [14], the hypernetwork adopts a simple MLP model with two 256-dimensional hidden layers and ReLU activation. The MLP first maps an input with $M + 2$ dimensions to a hidden embedding $\mathbf{h}(\lambda, \mathbf{w})$, which is then used to generate the decoder parameters by linear projection.

NHDE-M, deploying NHDE to MDRL [15], consists of three processes. In the meta-learning process, a meta-model θ_{meta} , whose architecture is the same as the HGA model θ , is trained by sampling tasks from the whole task space. In the fine-tuning process, according to the given λ and \mathbf{w} , θ_{meta} is then fine-tuned using fine-tuning instances with a few gradient steps to derive the corresponding submodel. In the inference process, the submodel is used to solve the corresponding subproblem.

C Node features and context embedding

The input dimensions of the node features vary with different problems. The inputs of the M -objective TSP are n nodes with $2M$ -dimensional features. The inputs of Bi-CVRP are n customer nodes with 3-dimensional features and a depot node with 2-dimensional features. The inputs of Bi-KP are n nodes with 3-dimensional features.

⁴ $r_i < \min\{f_i(\mathbf{x}) | \mathbf{f}(\mathbf{x}) \in \mathcal{F}\}$ and $z_i > \max\{f_i(\mathbf{x}) | \mathbf{f}(\mathbf{x}) \in \mathcal{F}\}$ for maximization problems, e.g., Bi-KP.

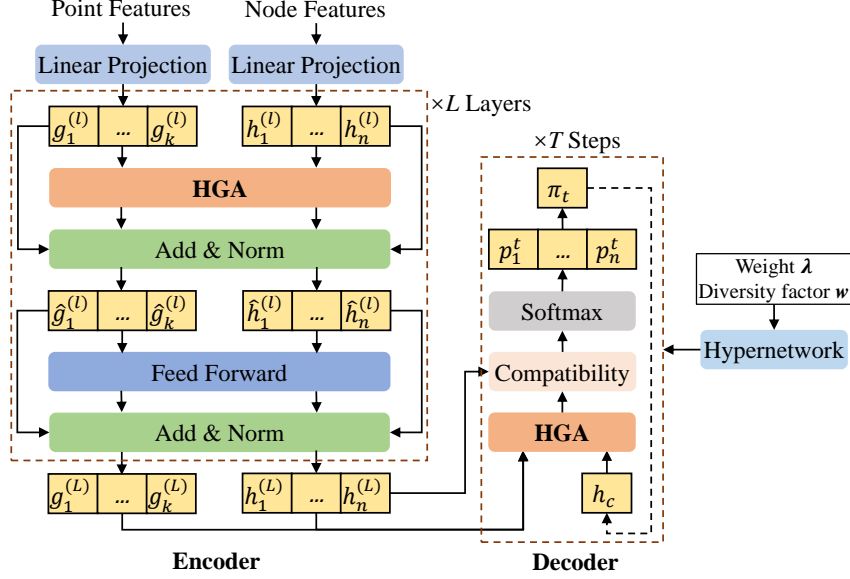


Figure 5: Hypernetwork-based heterogeneous graph attention (HGA) model of NHDE-P.

At step t in the decoder, a context embedding h_c is used to calculate the probability of node selection. For MOTSP, h_c is defined as the concatenation of the graph embedding $\bar{h} = \sum_{u=1}^n h_u/n$, the embedding of the first node h_{π_1} , and the embedding of the last node $h_{\pi_{t-1}}$. For MOCVRP, h_c is defined as the concatenation of the graph embedding \bar{h} , the embedding of the last node $h_{\pi_{t-1}}$, and the remaining vehicle capacity. For MOKP, h_c is defined as the concatenation of the graph embedding \bar{h} and the remaining knapsack capacity.

A masking mechanism is adopted in each decoding step to ensure the solution feasibility. For MOTSP, the visited nodes are masked. For MOCVRP (MOKP), besides the visited nodes, those with a demand (weight) larger than the remaining vehicle (knapsack) capacity are also masked.

D Instance augmentation

In the inference process, an instance can be transformed into other variants sharing the same optimal solutions, so as to augment the performance. An instance of Bi-CVRP has 8 transformations, and an instance of M -objective TSP has 8^M transformations [14] due to the full transformation permutation of M groups of 2-dimensional coordinates, where each group has 8 transformations [36], $\{(x, y), (1-x, y), (x, 1-y), (1-x, 1-y), (y, x), (1-y, x), (y, 1-x), (1-y, 1-x)\}$.

Our NHDE can effectively enhance the performance only using partial instance augmentation, which can reduce the solving time, since it can already achieve high diversity. Specifically, for M -objective TSP, NHDE adopts the full permutation of the first 4 transformations and last 4 transformations, respectively, thereby a total of 2×4^M transformations.

E Training and fine-tuning of NHDE-M

The training algorithm of NHDE-M in the meta-learning process, adapted from that of MDRL [15], is outlined in Algorithm 2. Also, the three key adjustments based on MDRL are captured in Line 7, Line 13, and Line 18. In the fine-tuning process, for the given N weights λ as well as diversity factors w , N submodels are fine-tuned from the well-trained meta-model to solve the MOCO problem. The fine-tuning algorithm is presented in Algorithm 3.

Algorithm 2 Training algorithm of NHDE-M

- 1: **Input:** weight distribution Λ , diversity-factor distribution \mathcal{W} , instance distribution \mathcal{S} , initial meta-learning rate ϵ_0 , number of meta-iterations T_m , number of sampling steps per meta-iteration N' , number of sampled weights per sampling step \tilde{N} , number of update steps of the submodel E , batch size B , instance size n
- 2: Initialize the meta-model θ
- 3: $\epsilon \leftarrow \epsilon_0$
- 4: **for** $t_m = 1$ to T_m **do**
- 5: $s_{e,i} \sim \text{SampleInstance}(\mathcal{S}) \quad \forall e \in \{1, \dots, E\} \quad \forall i \in \{1, \dots, B\}$
- 6: Initialize $\mathcal{F}_{e,i} \leftarrow \emptyset \quad \forall e, i$
- 7: **for** $n' = 1$ to N' **do**
- 8: **for** $\tilde{n} = 1$ to \tilde{N} **do**
- 9: $\lambda \sim \text{SampleWeight}(\Lambda)$
- 10: $w \sim \text{SampleDiversityFactor}(\mathcal{W})$
- 11: **for** $e = 1$ to E **do**
- 12: $\pi_i^j \sim \text{SampleSolution}(P_{\theta^{\tilde{n}}}(\cdot | s_{e,i}, \tilde{\mathcal{F}}_{r,e,i})) \quad \forall i \in \{1, \dots, B\} \quad \forall j \in \{1, \dots, n\}$
- 13: $R_i^j \leftarrow -w_1 g(\pi_i^j | s_{e,i}, \lambda) + w_2 \text{HV}_r(\tilde{\mathcal{F}}_{e,i} \cup \{\pi_i^j\}) \quad \forall i, j$
- 14: $b_i \leftarrow \frac{1}{n} \sum_{j=1}^n (-R_i^j) \quad \forall i$
- 15: $\nabla \mathcal{J}(\theta^{\tilde{n}}) \leftarrow \frac{1}{Bn} \sum_{i=1}^B \sum_{j=1}^n [(-R_i^j - b_i) \nabla_{\theta^{\tilde{n}}} \log P_{\theta^{\tilde{n}}}(\pi_i^j | s_i, \tilde{\mathcal{F}}_{r,i})]$
- 16: $\theta^{\tilde{n}} \leftarrow \text{Adam}(\theta^{\tilde{n}}, \nabla \mathcal{J}(\theta^{\tilde{n}}))$
- 17: $\mathcal{G}_i \leftarrow \{\pi_i^1, \dots, \pi_i^n\} \quad \forall i$
- 18: $\mathcal{F}_{e,i} \leftarrow \text{MPO}(\tilde{\mathcal{F}}_{e,i} \cup \tilde{\mathcal{G}}_i) \quad \forall e, i$
- 19: **end for**
- 20: **end for**
- 21: $\theta \leftarrow \theta + \epsilon (\frac{1}{\tilde{N}} \sum_{\tilde{n}=1}^{\tilde{N}} \theta^{\tilde{n}} - \theta)$
- 22: $\epsilon \leftarrow \epsilon - \epsilon_0 / (T_m \times N')$
- 23: **end for**
- 24: **end for**
- 25: **Output:** The parameter of the meta-model θ

Algorithm 3 Fine-tuning algorithm of NHDE-M

- 1: **Input:** instance distribution \mathcal{S} , weights $\lambda^1, \dots, \lambda^N$, diversity factors w^1, \dots, w^N , number of fine-tuning steps of the submodel E_f , batch size B , instance size n , well-trained meta-model θ
- 2: $s_{e,i} \sim \text{SampleInstance}(\mathcal{S}) \quad \forall e \in \{1, \dots, E_f\} \quad \forall i \in \{1, \dots, B\}$
- 3: Initialize $\mathcal{F}_{e,i} \leftarrow \emptyset \quad \forall e, i$
- 4: **for** $\tilde{n} = 1$ to N **do**
- 5: $\theta^{\tilde{n}} \leftarrow \theta$
- 6: **for** $e = 1$ to E **do**
- 7: $\pi_i^j \sim \text{SampleSolution}(P_{\theta^{\tilde{n}}}(\cdot | s_{e,i}, \tilde{\mathcal{F}}_{r,e,i})) \quad \forall i \in \{1, \dots, B\} \quad \forall j \in \{1, \dots, n\}$
- 8: $R_i^j \leftarrow -w_1 g(\pi_i^j | s_{e,i}, \lambda) + w_2 \text{HV}_r(\tilde{\mathcal{F}}_{e,i} \cup \{\pi_i^j\}) \quad \forall i, j$
- 9: $b_i \leftarrow \frac{1}{n} \sum_{j=1}^n (-R_i^j) \quad \forall i$
- 10: $\nabla \mathcal{J}(\theta^{\tilde{n}}) \leftarrow \frac{1}{Bn} \sum_{i=1}^B \sum_{j=1}^n [(-R_i^j - b_i) \nabla_{\theta^{\tilde{n}}} \log P_{\theta^{\tilde{n}}}(\pi_i^j | s_i, \tilde{\mathcal{F}}_{r,i})]$
- 11: $\theta^{\tilde{n}} \leftarrow \text{Adam}(\theta^{\tilde{n}}, \nabla \mathcal{J}(\theta^{\tilde{n}}))$
- 12: $\mathcal{G}_i \leftarrow \{\pi_i^1, \dots, \pi_i^n\} \quad \forall i$
- 13: $\mathcal{F}_{e,i} \leftarrow \text{MPO}(\tilde{\mathcal{F}}_{e,i} \cup \tilde{\mathcal{G}}_i) \quad \forall e, i$
- 14: **end for**
- 15: **end for**
- 16: **Output:** The parameters of the fine-tuned submodels $\theta^1, \dots, \theta^N$

F Hyperparameters of NHDE-M

NHDE-M trains a meta-model with 150 meta-iterations and initial meta-learning rate $\epsilon_0 = 1$. We set $N' = 20$, $\tilde{N} = M$, and $E = 100$. We use batch size $B = 64$ and the Adam [53] optimizer with

Table 5: Results of NHDE-M compared with MDRL with close or more total solving time on 200 random instances of MOCO problems.

Method	Bi-TSP20				Bi-TSP50				Bi-TSP100			
	HV↑	NDS ↑	Gap↓	Time	HV↑	NDS ↑	Gap↓	Time	HV↑	NDS ↑	Gap↓	Time
MDRL (40 wt.)	0.6264	20	0.49%	2s	0.6342	33	1.35%	3s	0.6940	36	1.55%	8s
MDRL (600 wt.)	<u>0.6287</u>	54	<u>0.13%</u>	29s	0.6380	133	0.76%	64s	0.7006	185	0.61%	2.1m
NHDE-M (40 wt.)	<u>0.6287</u>	58	<u>0.13%</u>	20s	0.6393	132	0.56%	57s	0.7008	195	0.58%	2.0m
MDRL (40 wt. aug.)	0.6267	18	0.44%	21s	0.6384	34	0.70%	1.5m	0.6995	38	0.77%	3.3m
MDRL (100 wt. aug.)	0.6271	23	0.38%	1.2m	<u>0.6408</u>	67	<u>0.33%</u>	3.6m	<u>0.7023</u>	82	<u>0.37%</u>	16m
NHDE-M (40 wt. aug.)	0.6295	81	0.00%	1.5m	0.6429	273	0.00%	2.6m	0.7049	339	0.00%	5.5m
Method	Bi-CVRP20				Bi-CVRP50				Bi-CVRP100			
	HV↑	NDS ↑	Gap↓	Time	HV↑	NDS ↑	Gap↓	Time	HV↑	NDS ↑	Gap↓	Time
MDRL (40 wt.)	0.4284	9	0.49%	3s	0.4057	5	1.12%	5s	0.4015	0	1.45%	10s
MDRL (300 wt.)	0.4296	17	0.21%	23s	<u>0.4089</u>	21	<u>0.34%</u>	49s	<u>0.4078</u>	21	<u>-0.10%</u>	1.5m
NHDE-M (40 wt.)	0.4296	16	0.21%	23s	0.4086	20	0.41%	47s	0.4053	18	0.52%	1.4m
MDRL (40 wt. aug.)	0.4293	9	0.28%	5s	0.4073	11	0.73%	16s	0.4040	11	0.83%	1.0m
MDRL (300 wt. aug.)	<u>0.4302</u>	16	<u>0.07%</u>	1.0m	0.4103	24	0.00%	2.1m	0.4086	24	-0.29%	7.7m
NHDE-M (40 wt. aug.)	0.4305	24	0.00%	1.2m	0.4103	29	0.00%	1.6m	0.4074	26	0.00%	2.7m
Method	Bi-KP50				Bi-KP100				Bi-KP200			
	HV↑	NDS ↑	Gap↓	Time	HV↑	NDS ↑	Gap↓	Time	HV↑	NDS ↑	Gap↓	Time
MDRL (40 wt.)	0.3559	17	0.20%	4s	0.4528	25	0.31%	8s	0.3594	31	0.42%	24s
MDRL (300 wt.)	<u>0.3563</u>	29	<u>0.08%</u>	30s	<u>0.4536</u>	58	<u>0.13%</u>	1.0m	<u>0.3606</u>	95	<u>0.08%</u>	3.1m
NHDE-M (40 wt.)	0.3566	41	0.00%	31s	0.4542	93	0.00%	1.0m	0.3609	160	0.00%	2.8m
Method	Tri-TSP20				Tri-TSP50				Tri-TSP100			
	HV↑	NDS ↑	Gap↓	Time	HV↑	NDS ↑	Gap↓	Time	HV↑	NDS ↑	Gap↓	Time
MDRL (210 wt.)	0.4723	126	0.90%	14s	0.4388	199	4.46%	20s	0.4956	207	3.17%	40s
MDRL (3003 wt.)	0.4761	479	0.10%	2.6m	<u>0.4512</u>	1927	<u>1.76%</u>	5.1m	<u>0.5104</u>	2400	<u>0.27%</u>	10m
NHDE-M (210 wt.)	<u>0.4763</u>	783	<u>0.06%</u>	1.4m	<u>0.4512</u>	2636	<u>1.76%</u>	4.7m	0.4997	4056	2.36%	11m
MDRL (210 wt. aug.)	0.4727	107	0.82%	14m	0.4473	202	2.61%	53m	0.5056	209	1.21%	4.3h
MDRL (153 wt. aug.)	0.4721	92	0.94%	11m	0.4448	150	3.16%	39m	0.5022	153	1.88%	3.2h
NHDE-M (210 wt. aug.)	0.4766	748	0.00%	13m	0.4593	10850	0.00%	30m	0.5118	13216	0.00%	1.5h

learning rate 10^{-4} . During fine-tuning and inference, the number of fine-tuning steps E_f is set to 50, and Adam with learning rate 10^{-4} is used. $N = 40$ and $N = 210$ uniformly distributed weights are generated and then shuffled for $M = 2$ and $M = 3$, respectively. N diversity factors linearly change from (1,0) to (0,1). For the compared MDRL, the settings are the same as NHDE-M except 3000 meta-iterations are used, so that MDRL and NHDE-M execute the same number of gradient steps.

G Experimental results of NHDE-M

G.1 More results of NHDE-M

NHDE-M usually spends relatively more inference time than MDRL with the same number of weights. Hence, we adjust the number of weights of MDRL, making its inference time close to or longer than NHDE-M for fair comparisons, as shown in Table 5. Nonetheless, NHDE-M is still superior to MDRL in most cases. Without instance augmentation (aug.), NHDE-M is inferior to MDRL on Bi-CVRP50, Bi-CVRP100, and Tri-TSP100. Instance augmentation can effectively boost the performance of NHDE-M, where NHDE-M (aug.) is only inferior to MDRL (aug.) on Bi-CVRP100. Note that, for a given weight, MDRL needs to further fine-tune the meta-model with $E_f = 50$ gradient steps to derive a submodel to the corresponding subproblem, which means that the increasing number of weights would cause considerable extra fine-tuning costs.

G.2 Generalization study of NHDE-M

We assess the zero-shot generalization capability of NHDE-M, which is trained and fine-tuned on Bi-TSP100, and tested on 200 random larger-scale Bi-TSP instances, i.e., Bi-TSP150/200, and three commonly used benchmark instances, i.e., KroAB100/150/200. The results are gathered in Tables 6 and 7. The Pareto fronts of the benchmark instances obtained by various methods are also visualized

Table 6: Results of NHDE-M on 200 random instances of larger-scale problems.

Method	Bi-TSP150				Bi-TSP200			
	HV↑	NDS ↑	Gap↓	Time	HV↑	NDS ↑	Gap↓	Time
WS-LKH (40 wt.)	0.7075	39	-0.90%	5.3h	0.7435	40	-1.38%	8.5h
PPLS/D-C (200 iter.)	0.6784	473	3.25%	21h	0.7106	512	3.11%	32h
DRL-MOA (101 models)	0.6901	73	1.58%	45s	0.7219	75	1.57%	87s
MDRL (40 wt.)	0.6894	37	1.68%	23s	0.7227	38	1.46%	42s
MDRL (400 wt.)	0.6958	176	0.77%	3.7m	0.7284	190	0.68%	6.9m
NHDE-M (40 wt.)	0.6970	239	0.60%	3.0m	0.7297	268	0.50%	4.1m
MDRL (40 wt. aug.)	0.6948	39	0.91%	21m	0.7275	39	0.80%	41m
NHDE-M (40 wt. aug.)	<u>0.7012</u>	373	<u>0.00%</u>	14m	<u>0.7334</u>	395	<u>0.00%</u>	25m

Table 7: Results of NHDE-M on benchmark instances.

Method	KroAB100				KroAB150				KroAB200			
	HV↑	NDS ↑	Gap↓	Time	HV↑	NDS ↑	Gap↓	Time	HV↑	NDS ↑	Gap↓	Time
WS-LKH (40 wt.)	0.7007	40	-0.42%	53s	0.6989	39	-0.92%	1.9m	0.7404	40	-1.48%	2.2m
PPLS/D-C (200 iter.)	0.6785	388	2.77%	31m	0.6659	441	3.84%	1.1h	0.7100	491	2.69%	3.1h
DRL-MOA (101 models)	0.6903	67	1.07%	10s	0.6794	72	1.89%	18s	0.7185	73	1.52%	23s
MDRL (40 wt.)	0.6869	37	1.56%	5s	0.6810	36	1.66%	9s	0.7184	39	1.54%	12s
NHDE-M (40 wt.)	0.6940	183	0.54%	7s	0.6879	232	0.66%	12s	0.7253	275	0.59%	16s
MDRL (40 wt. aug.)	0.6928	37	0.72%	7s	0.6857	38	0.98%	10s	0.7234	40	0.85%	15s
NHDE-M (40 wt. aug.)	<u>0.6978</u>	341	<u>0.00%</u>	10s	<u>0.6925</u>	370	<u>0.00%</u>	12s	<u>0.7296</u>	393	<u>0.00%</u>	16s

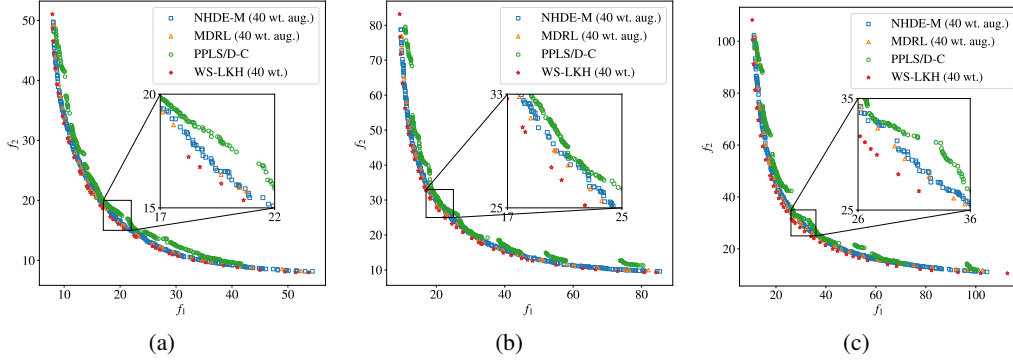


Figure 6: Pareto fronts of NHDE-M and compared methods on benchmark instances. (a) KroAB100. (b) KroAB150. (c) KroAB200.

in Figure 6. As can be clearly observed, NHDE-M exhibits superior generalization capability to the state-of-the-art MOEA and other neural methods with regard to the convergence and diversity.

H Detailed results of NHDE-P on benchmark instances

Table 8 records the detailed results of NHDE-P and other baselines on benchmark instances, which demonstrate the superiority of NHDE-P.

I Details of compared methods in ablation study

In Figure 4(a), we compare NHDE-P with decomposition-based DRL without indicator (NHDE w/o I) and indicator-based DRL without decomposition (NHDE w/o D) to study the effect of the indicator-enhanced DRL. Concretely, NHDE w/o I removes the HV indicator in the reward and the Pareto front graph in the inputs. NHDE w/o D dispenses with weights, removes the scalar objective in the reward, and only adopts the HV indicator to guide the model. In each subproblem without a weight, a new solution (or multiple sampled solutions) is produced to maximize the HV indicator

Table 8: Results of NHDE-P on benchmark instances.

Method	KroAB100				KroAB150				KroAB200			
	HV↑	NDS ↑	Gap↓	Time	HV↑	NDS ↑	Gap↓	Time	HV↑	NDS ↑	Gap↓	Time
WS-LKH (40 wt.)	0.7007	40	-0.47%	53s	0.6989	39	-0.92%	1.9m	0.7404	40	-1.58%	2.2m
PLS/D-C (200 iter.)	0.6785	388	2.71%	31m	0.6659	441	3.84%	1.1h	0.7100	491	2.59%	3.1h
DRL-MOA (101 models)	0.6903	67	1.02%	10s	0.6794	72	1.89%	18s	0.7185	73	1.43%	23s
PMOCO (40 wt.)	0.6862	36	1.61%	7s	0.6802	37	1.78%	9s	0.7174	38	1.58%	12s
NHDE-P (40 wt.)	0.6926	179	0.69%	8s	0.6873	225	0.75%	12s	0.7247	246	0.58%	16s
PMOCO (40 wt. aug.)	0.6916	38	0.83%	8s	0.6861	37	0.92%	11s	0.7223	39	0.91%	16s
NHDE-P (40 wt. aug.)	0.6974	317	0.00%	11s	0.6925	365	0.00%	13s	0.7289	377	0.00%	17s

Table 9: Results with change of the number of weights.

Number of wt.		Time		HV		NDS	
NHDE-P	PMOCO	NHDE-P	PMOCO	NHDE-P	PMOCO	NHDE-P	PMOCO
10	150	14s	14s	0.6334	0.6355	76	56
20	300	26s	26s	0.6373	0.6359	103	63
40	600	53s	53s	0.6388	0.6361	127	68
80	1200	1.3m	1.4m	0.6395	0.6362	146	70

Table 10: Results for the runtime proportion of each module.

Module of NHDE-P	Runtime Proportion
PMOCO	13%
Indicator-enhanced inference	5%
MPO	82%

under the current Pareto front. The surrogate landscape cannot be defined due to the disuse of weights, so the current whole Pareto front is taken as the input to the model.

Since HV can comprehensively measure convergence and diversity, indicator-based NHDE w/o D should find a Pareto set with good overall performance in intuition. However, it is even inferior to decomposition-based NHDE w/o I in practice. This fact reveals that it is difficult for the deep model to learn to construct solutions to directly optimize HV due to the high complexity of HV.

With respect to NHDE w/o MPO, which is used to evaluate the impact of our MPO strategy, it still samples multiple solutions for each subproblem, but only the solution with the maximum reward is preserved according to the view of single-objective optimization.

J Runtime analysis

We provide the NHDE and PMOCO results on Bi-TSP50 with similar runtime, by changing the number of weights used in both methods in Table 9. When using a few weights (short runtime), PMOCO is slightly better than NHDE with close runtime (since the increasing number of weights can rapidly raise the performance of PMOCO). However, when using more weights ($N \geq 300$ for PMOCO), NHDE is consistently better than PMOCO with a close runtime. This further verifies that increasing weights may not effectively produce more Pareto solutions for existing neural solvers, while our NHDE can boost the limitation of such decomposition-based neural solvers, especially in diversity. The superiority is more significant for larger and more complex MOCVRP instances.

Moreover, we present the runtime proportion of each module in NHDE-P, including the original PMOCO, indicator-enhanced DRL, and MPO. The experiment is conducted on Bi-TSP50, as shown in Table 10. Please note that the runtime of the indicator-enhanced DRL during inference is mainly spent by the heterogeneous graph attention (HGA). The indicator-enhanced inference costs 5% runtime, with the complexity of the attention mechanism in PMOCO being $O(n^2)$ and the additional complexity in HGA being $O(nK)$. MPO costs 82% runtime, since the update of Pareto front needs more computation, i.e., $O((K + J)J)$.

Table 11: Comparison on NHDE-P with NHDE w/o I when using much more weights.

Method	HV	NDS	Time
NHDE-P (600 wt.)	0.6405	177	6.3m
NHDE w/o I (600 wt.)	0.6372	141	5.9m

We observe that the promising performance of NHDE comes more from MPO (see NHDE w/o MPO with HV 0.6335 in Figure 4(a)) than the indicator-enhanced inference (see NHDE w/o I with HV 0.6361 in Figure 4(a)). As presented in Table 10, the indicator-enhanced inference only costs a very small part of runtime, while MPO costs most of the runtime. Thus, their corresponding contributions to performance are reasonable, considering their computational efforts.

We also compare NHDE-P with NHDE w/o I (equivalent to PMOCO with MPO) when using much more weights (i.e., 600) on Bi-TSP50. As shown in Table 11, our NHDE outperforms PMOCO with MPO, where PMOCO spends similar runtime to NHDE with the extra MPO module.

K Weight assignment

Recall that we use uniformly distributed weights during inference, which is a mainstream method for weight assignment when no information about the Pareto front is known in advance. For decomposition-based methods, weight assignment methods may affect the solution distribution. However, our NHDE can better alleviate this issue compared with pure decomposition-based neural heuristics for two reasons: (1) NHDE can generate more diverse solutions as verified by our experiments. (2) NHDE can also flexibly handle arbitrary weights during inference, enabling it to integrate seamlessly with proper weight assignment methods. When knowing the approximate scales of different objectives beforehand, we can first normalize them into $[0,1]$ to derive a more uniform Pareto front. Otherwise, we can assign biased and non-uniform weights during inference to obtain more uniformly distributed solutions.

We present the results on Tri-TSP with asymmetric Pareto fronts, as shown in Figure 7. For Tri-TSP instances, the coordinates for the three objectives are randomly sampled from $[0, 1]^2$, $[0, 0.5]^2$, $[0, 0.1]^2$, respectively. The results show that non-uniform weights, which are obtained by multiplying uniform weights by (1,2,10) element-wise and then normalizing them back to $[0, 1]^3$, can produce a relatively more uniform Pareto front. Besides, compared with PMOCO (see Figure 7(b)), NHDE-P (see Figure 7(c)) can enhance diversity, thereby alleviating the non-uniform distribution of solutions.

L Hyperparameter study

We further study the effects of N' (the number of weights used in training), K (the limited size of the surrogate landscape of the Pareto front), and J (the limited number of *points* from new solutions for updating the Pareto front).

We present the results of various N' on Bi-TSP50 in the table below. As shown in Figure 8(a), $N' = 5$ and $N' = 10$ cause inferior performance, while proper N' ($20 \leq N' \leq 40$) results in desirable performance. Intuitively, when limiting the same total gradient steps in training, a larger N' means fewer instances used for model training. In this sense, too large N' , i.e., with insufficient instances, could lead to the inferior performance for solving unseen instances. On the other hand, too small N' could prevent the model from learning favorable weight representations and thus deteriorate the final performance. Hence we choose $N' = 20$ in this paper.

Figure 8(b) displays the results of various values of K , where $K = 20$ is a desirable setting. When K is too small, some key information of the Pareto front would be lost, thereby degrading the performance. When K is too large, the deep model cannot cope with numerous points of the Pareto front, also leading to deterioration of the performance.

We provide the HV and runtime of NHDE-P on Tri-TSP50 with the changed J in Figure 8(c). We observe that by limiting J , the massive time of the update can be curtailed with only a little sacrifice of performance. Since $J = 200$ is a good trade-off between HV and runtime, we use it in this paper.

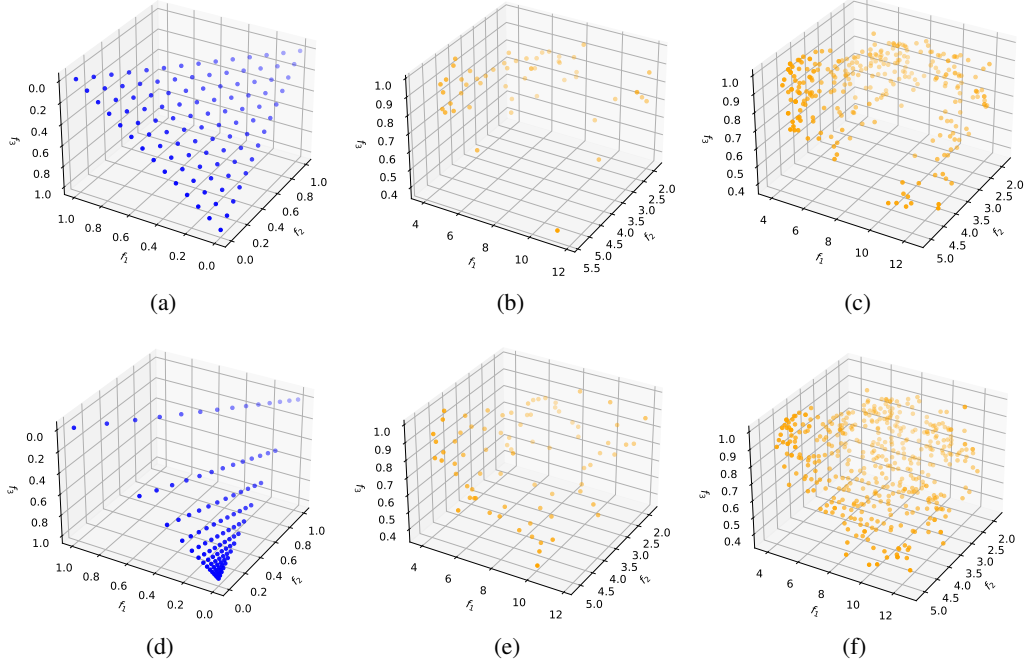


Figure 7: Solutions generated by using 105 uniform/non-uniform distributed weights on an instance of Tri-TSP20 with asymmetric Pareto front. (a) Uniform weights. (b) PMOCO with uniform weights. (c) NHDE-P with uniform weights. (d) Non-uniform weights. (e) PMOCO with non-uniform weights. (f) NHDE-P with non-uniform weights.

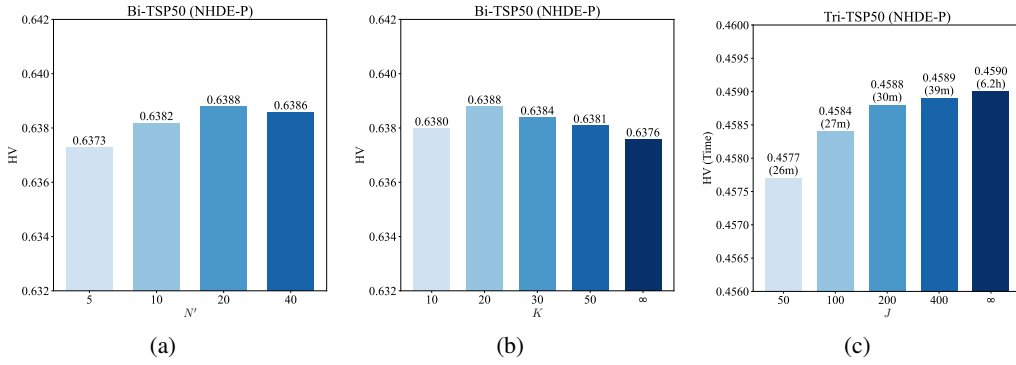


Figure 8: Hyperparameter study. (a) Effect of the number of weights used in training. (b) Effect of the limited size of the surrogate landscape of the Pareto front. (c) Effect of the limited number of *points* from new solutions for updating the Pareto front.

M Additional analysis

In the inference, diversity factors are linearly changed, which means different emphasis between the scalar objective and the HV indicator. We test other settings of the diversity factors, e.g., some fixed values. As shown in Figure 9(a), different settings of the diversity factors have almost no impact on the performance, except $w^1 = \dots = w^N = (1, 0)$ only emphasizing on HV. A possible reason is that the deep model is not good at learning the mapping from diversity factors to the complicated reward involving HV.

Recall that NHDE solves the subproblems dependently, and we simply use the shuffled weights. To study the effect of the random shuffle, we execute independent 10 runs. The boxplot of the results is

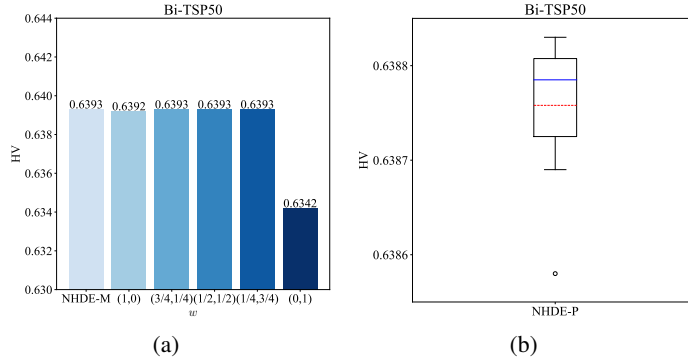


Figure 9: Additional analysis. (a) Effect of diversity factors. (b) Effect of shuffled weights.

Table 12: Results for the number of duplicated solutions.

Method	DS
NHDE-P (40 wt.)	196
NHDE w/o I (40 wt.)	225

Table 13: Variances of the methods.

Method	Bi-TSP20		Bi-TSP50		Bi-TSP100	
	HV	Variance	HV	Variance	HV	Variance
WS-LKH (40 wt.)	0.6266	3.24×10^{-4}	0.6402	1.59×10^{-4}	0.7072	4.82×10^{-5}
PPLS/D-C (200 iter.)	0.6256	3.45×10^{-4}	0.6282	1.72×10^{-4}	0.6844	6.13×10^{-5}
DRL-MOA (101 models)	0.6257	3.31×10^{-4}	0.6360	1.67×10^{-4}	0.6970	5.09×10^{-5}
PMOCO (40 wt.)	0.6258	3.31×10^{-4}	0.6331	1.64×10^{-4}	0.6938	5.08×10^{-5}
PMOCO (600 wt.)	0.6267	3.28×10^{-4}	0.6361	1.55×10^{-4}	0.6978	4.71×10^{-5}
NHDE-P (40 wt.)	0.6286	3.19×10^{-4}	0.6388	1.58×10^{-4}	0.7005	4.76×10^{-5}
PMOCO (40 wt. aug.)	0.6266	3.26×10^{-4}	0.6377	1.60×10^{-4}	0.6993	4.99×10^{-5}
PMOCO (100 wt. aug.)	0.6270	3.28×10^{-4}	0.6395	1.54×10^{-4}	0.7016	4.81×10^{-5}
NHDE-P (40 wt. aug.)	0.6295	3.14×10^{-4}	0.6429	1.52×10^{-4}	0.7050	4.73×10^{-5}

presented in Figure 9(b). As shown, the random shuffle of weights only exhibits a slight impact on the performance. A specialized order of the weights may raise the performance, but it is beyond the scope of this paper, which would be explored in the future.

We implicitly show the reduced duplicated solutions by the metric $|NDS|$, i.e., the number of non-dominated solutions. Empirically, more non-dominated solutions mean fewer duplicated solutions and fewer dominated solutions. Thus, the larger $|NDS|$ values of our method (especially in comparison to the other neural solvers) indicate that our method can produce a smaller number of duplicates to some extent. Furthermore, we add another evidence to verify that the indicator-enhanced DRL can hinder duplicated solutions. Specifically, we directly report the average number of duplicated solutions ($|DS|$) of our NHDE-P and NHDE-P without indicator (NHDE w/o I) on Bi-TSP50 in Table 12. As can be seen, our NHDE-P using the HV indicator can effectively guide the model to generate fewer duplicated solutions. Intuitively, our model is trained to construct new Pareto solutions different from existing ones in the Pareto front, which could achieve higher HV in the reward.

To further verify our results are statistically significant, we have conducted a Wilcoxon rank-sum test at a 1% significance level for the results in all groups, which means our results are statistically significant. We additionally report the variances of the results in Table 13. All methods have small variances of hypervolumes, where our NHDE-P achieves the stablest performance.